# Bubble size distribution measurement, modeling and control in a laboratory flotation column

**Mémoire**

**Alberto Riquelme-Diaz**

**Maîtrise en génie électrique**
Maître ès sciences (M.Sc.)

Québec, Canada

# Résumé

Ce travail de recherche vise à mesurer et à contrôler la distribution du diamètre des bulles (DDB) dans une colonne de flottation. L'objectif se décompose en trois parties.

La première phase vise à estimer correctement la taille des bulles grâce à des algorithmes de traitement d'images prises par une caméra. La DDB obtenue est ensuite modélisée par une distribution log-normale qui est définie par deux paramètres, la moyenne et l'écart type.

Deuxièmement, grâce au nouveau système de mesure et à la représentation log-normale, un modèle dynamique à gains non linéaires (structure de Wiener) dont les sorties sont la moyenne et l'écart-type de la DDB est estimé. Une bonne concordance entre la réponse du système expérimental et celle du modèle identifié est observée.

Finalement, une stratégie de commande prédictive contrainte basée sur le modèle de Wiener est conçue afin de réguler la BSD. Les résultats de laboratoire obtenus sont très satisfaisants.

# Abstract

This research aims to measure and control the bubble size distribution (BSD) in a flotation column. The objective is divided into three parts.

The first phase is to correctly estimate the bubble size using algorithms processing images taken by a camera. The obtained BSD is then modeled by a log-normal distribution which is defined by two parameters, its mean and standard deviation.

Second, thanks to the new measurement system and the log-normal representation, a dynamic model with nonlinear gains (Wiener structure) whose outputs are the mean and standard deviation of the DDB is estimated. Good agreement between the response of the pilot system and the response of the identified model is observed.

Finally, a constrained predictive controller based on the Wiener model is designed to regulate the BSD. Laboratory results obtained are very satisfactory.

# Contents



[1] A. Riquelme, A. Desbiens, R. del Villar, and M. Maldonado. "A device for measuring conductivity of dispersions". Measurements, 59:49-55, 2014

[2] A. Riquelme, J. Bouchard, A. Desbiens and R. del Villar. "Bubble detection in flotation columns based

on cicular Hough transform". World Mining Congress, 1:2-10, 2013

[3] A. Riquelme, A. Desbiens, R. del Villar, and M. Maldonado. "Non-linear bubble size distribution modeling in a flotation column". This article is in process of submission to the International Journal of Mineral Processing.

[4] A. Riquelme, A. Desbiens, R. del Villar, and M. Maldonado. "Bubble Size Distribution control in a flotation column". This article is in process of submission to the journal Minerals Engineering.

# List of Tables

# List of Figures

*To my loved ones*

All in all you were all just bricks
in the wall.

---

Pink Floyd

# Acknowledgements

I am using this opportunity to express my gratitude to everyone who supported me throughout the course of this research. I am thankful for their aspiring guidance, invaluably constructive criticism and friendly advice during the project work. I am sincerely grateful to them for sharing their truthful and illuminating views on a number of issues related to the project.

I express my warm thanks to Mr. Desbiens, Mr. del Villar and Mr. Maldonado for their support and guidance. Also to Mr. Eric Poulin and Mr. Joselyn Bouchard for their help and advises.

I have to acknowledge all my colleagues in the LOOP for their assistances in many aspects that I cannot list them all because of limited space. They are Ricardo Esteban, Danny Calisaya, Carole Prevoste, Yanick Beaudoin, Soufiane Hallab, Amir Vasebi and Ali Vazirizadeh. I also thanks to the Electric department and the mining and metallurgy department personnel for their help and friendship.

Last but not the least important, I owe more thanks to my family. Words cannot express how grateful I am to my mother and father for all of the sacrifices that you've made on my behalf. Also I would like to thank to my brother and sister for their endless support. I would also like to thank all of my friends who colored my life during these years. At the end I would like express appreciation to my dear Marika who supported me in my decisions, for her encouragement and editing assistance. My heartfelt thanks to everyone.

# Avant-propos

- Le chapitre 3 est l'article *A device for measuring conductivity of dispersions* [78], publié le 6 Mars 2014 dans la revue Measurements et dont les auteurs sont Alberto Riquelme, André Desbiens, René del Villar et Miguel Maldonado. Les travaux décrits dans cet article n'ont pas été realisés dans le cadre de cette maîtrise mais dans un projet antérieur. Toutefois, l'écriture de l'article est un des travaux réalisés dans le cadre de cette maîtrise. Mon rôle dans l'écriture de l'article en tant qu'auteur principal était la rédaction de l'article, supervisée par les co-auteurs pour les corrections.

- Le chapitre 4 est formé de sections tirées de l'article *Bubble detection in flotation columns based on circular Hough transform* [76], accepté et presenté par moi-même à la conférence 23rd World Mining Congress, Montréal, Québec, Canada, du 11 au 15 Août 2013. J'ai participé à la rédaction de l'article à titre de premier auteur, suivi par les professeurs Jocelyn Bouchard, André Desbiens et Rene del Villar qui ont contribué à l'édition de ce document. La conception générale de la technique de mesure et la totalité des analyses en laboratoire ont été réalisées par moi-même sous la supervision de M. Desbiens et M. del Villar.

- Le chapitre 5 correspond à l'article *Non-linear bubble size distribution modeling in a flotation column.* Les sections décrivant le fonctionnement d'une colonne de flottation, le montage expérimental et l'analyse d'images ont été retirées afin d'éviter des répétitions. Les auteurs sont Alberto Riquelme, André Desbiens, Rene del Villar et Miguel Maldonado. Cet article sera bientôt soumis au International Journal of Mineral Processing. La conception générale de la stratégie de mesure et l'identification du modèle Wiener ainsi que la totalité des analyses en laboratoire ont été réalisées par moi-même sous la supervision de M. Desbiens et M. del Villar. J'ai participé à la rédaction de l'article à titre de premier auteur, suivi par les autres auteurs qui ont contribué à l'édition de ce document.

- Le chapitre 6 correspond à l'article *Bubble Size Distribution control in a flotation column.* Les sections décrivant le fonctionnement d'une colonne de flottation, le montage expérimental et la modélisation du système ont été retirées afin d'éviter des répétitions. Cet article sera bientôt soumis au Minerals Engineering. Les auteurs sont Alberto Riquelme,

André Desbiens, Rene del Villar et Miguel Maldonado. J'ai participé à la conception, à l'application et à la conduite des tests pour évaluer la performance de cette stratégie de contrôle sous la direction du professeur Desbiens. J'ai participé à la rédaction de l'article à titre de premier auteur, suivi par les autres auteurs qui ont contribué à l'edition de ce document.

Directeur: André Desbiens.

# Chapter 1

# Introduction

Flotation is a method used to separate valuable minerals from useless ones (gangue) by mean of a differential behavior with respect to air bubbles. The devices where this process takes place are of two types: mechanical cells where pulp is suspended by an agitator and pneumatic cells using air for this task. The flotation column, the most common device of this latter category, consists of a tall cylindrical vessel where a slurry of finely ground minerals is introduced at about 80% of its height. Air is injected at the bottom part, where it is dispersed into fine bubbles by using a device called "sparger". Besides collecting particles, this flow of rising bubbles also helps keeping the particles in suspension. In order to provide the required air flow rate into the industrial columns, an array of several spargers is usually implemented. Prior to its admission to the column, the slurry is usually conditioned with chemicals that render hydrophobic the surface of valuable minerals (target metal containing particles) and consequently be able to attach to the rising bubbles. As a result of the difference in specific gravity between pulp and bubble-particle aggregates, these latter reach the top of the column, forming a froth rich in valuable minerals. The overflow, leaving the cell at the top of the column, is usually the valuable product, called concentrate. On the other hand, the gangue (generally the non-valuable minerals) leaves the column through the bottom part of the column in a stream called tailings. This flotation process is called direct flotation. In some cases, the tailings may constitute the product rich in valuable minerals and the concentrate is the non-desired product. This operation is called inverse flotation. This is the case when a high mineral grade pulp with little gangue content is to be separated. For example, to enrich a mineral containing 95% of hematite (valuable mineral) and 5% of silica (gangue), is more economical to add a reagent to make the silica hydrophobic and to collect it as a concentrate, while the hematite enriched product is collected as tailings.

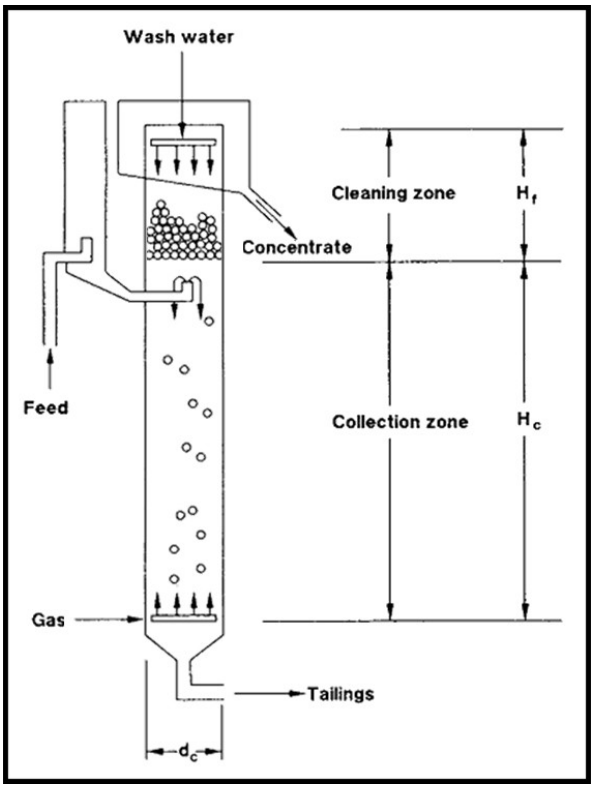


Figure 1.1: Schematic representation of a flotation column [22].

## 1.1 Process description

Flotation columns were introduced in the early 60s [93] and they were first successfully implemented for industrial mineral separation in 1981 [14], showing a good performance in producing clean concentrates and good recoveries. Since then, column flotation has gained in popularity, being presently a standard flotation device in the mineral processing industry, particularly in concentrate cleaning stages. Their success is related to less physical space, good concentrate grades, less instrumentation and maintenance, less energy consumption, etc [14].

Most columns are of a circular section, around 3 m in diameter and 10 m to 14 m in height. A schematic representation of a flotation column is shown in Figure 1.1 [22]. A previously conditioned (for mineral hydrophobisation) slurry stream is fed at around 1 to 2 m from the top of the column, while a gas flow (usually air) is injected at the bottom via a sparging device. Under normal operating conditions, two different zones are distinguished. The lower zone, between the feed inlet and the sparger is called the pulp zone or collection zone, since it is here that the collection of particles by bubbles takes place. It typically contains less than 20-30% of air (volume fraction). The second zone, between the feed port and the top of the column, is called the froth zone or the cleaning zone. This section contains a much greater air fraction, typically above 70%.

A distinctive characteristic of flotation columns is the addition of a fine spray of water above the overflowing concentrate. In normal operating conditions, a fraction of this water travels though the froth zone. This stream washes down any hydrophilic particle that could have been hydraulically entrained with the rising bubbles, thus improving the concentrate grade. Also, this downward water flow helps the froth stabilization. The remaining fraction of wash water overflows the column helping the removal of the concentrate.

Since almost all minerals are naturally hydrophilic, their hydrophobisation is necessary prior to their admission to the column. The feed slurry is then conditioned in an ad-hoc vessel (conditioner) with ad-hoc chemicals rendering hydrophobic the surface of the valuable minerals (target metal containing particles) and consequently enabling them to attach to the rising bubbles. Various reagents are generally required: collectors, activators, depressants and pH modifiers. Even though some of these chemicals are normally added in a preliminary stage (conditioner), they may be directly added into the flotation device (cell or column); this is particularly the case of the frother. The addition of collectors, depressants and pH modifiers plays an important role on the metallurgical performance since it will determine the ability of the desired particles to be collected by the rising bubbles and leave the column as concentrate.

Laurila et al. [46] suggested that the following variables are the most important from a flotation control viewpoint:

- slurry properties (density, solids content)
- slurry flow rate (retention time)
- electrochemical parameters/potentials (pH, Eh, conductivity)
- chemical reagents and their dosage (frothers, collectors, depressants, activators)
- pulp level in the cells
- air flow rate added to the cells
- froth properties (speed, bubble size distribution, froth stability)
- particle properties (size distribution, shape, degree of mineral liberation)
- mineralogical composition of the ore
- mineral concentrations in the feed, concentrate and tailings (recovery, grade)
- froth wash water rate (especially in flotation columns)

Assuming that pulp has already been conditioned in a previous stage, cell/column pulp level, froth properties, gas dispersion properties and froth wash water rate are the only variables

that can be controlled inside the flotation column. The process variables involved inside the flotation cell/column are called froth depth, bias rate, gas rate, gas hold up, bubble size and bubble surface area flux. The last three variables are part of the gas dispersion properties, and they partially modify the hydrodynamic properties inside the column, affecting directly the metallurgical performance. Consequently, most recent research has been centered on monitoring and controlling gas dispersions properties as a key towards flotation optimization. Flotation column variables will be described in more detail in the following section.

## 1.2 Process variables

### 1.2.1 Froth depth

Froth depth ($H_f$) is defined as the distance between the top of the column (concentrate overflow) and the actual position of the pulp-froth interface. It determines the height of cleaning and collection zones and therefore the pulp residence time in the collection zone. This variable contributes to the value of the recovery in collection zone. It is closely monitored and controlled in industrial plants by different methods (pressure transmitter methods, ultrasonic methods, float methods, conductivity profile, etc.) and is usually controlled manipulating the tailing flow, either with a pump or a pinch valve.

In flotation columns, froth depth can vary between 20 and 150 cm. It mainly depends on the column total height, the type of mineral to be extracted, its particle size and previous conditioning stages. A shallow $H_f$ allows a bigger recovery (less drop-back), while the grade is reduced (not sufficient cleaning effect). The inverse case, a deep $H_f$, reduces recovery but increases the concentrate grade. In general, the use of a specific froth depth will depend somehow on the existing degree of gangue entrainment.

### 1.2.2 Bias rate

Bias rate ($J_b$) refers to the fraction of the wash water stream going through the cleaning zone. More precisely, it is defined as the net downward flow of water crossing the interface per cross sectional area of the column [22]. It is an index for measuring the performance of the added wash water in cleaning the froth zone. The amount of wash water going through the froth zone cleans the concentrate from entrained hydrophilic particles and stabilizes the froth zone, allowing to increase the froth depth if needed. Bias is said to be positive if water moves downward the column, and negative otherwise [22]. A negative bias would decrease the concentrate grade, since part of the feed will join the concentrate, which is not a desirable condition. The optimal value of bias rate have been discussed by different research groups. While some claim that a small bias rate is enough to ensure the cleaning action [22], others have established that small bias values do not have an important influence on the concentrate grade [15]. Nevertheless, there is a common agreement in that a high bias rate has a negative

influence on the process, degrading the froth stability [105]. Under steady-state conditions, the bias could be directly calculated by doing a water balance inside the column. This method uses the mass balance between the feed, the wash water and the tail to calculate the fraction of wash water that goes to the tail. For computing these water streams it is necessary to measure the flow rate and the percentage of solids of feed and tail streams. This requires two magnetic flow meters to measure the superficial velocity and two $\gamma$-ray density meters to measure the percentage of solid [54]. The resulting accuracy is poor given that four measurements are taken on two large streams to calculate a very small value (bias).

Another method, based on conductivity, was proposed by Maldonado et al. [54]. It uses the Maxwell equation [60] for mixture of electrolytes, to calculate the fraction of wash water that crosses the interface, which is representative of the bias. To use this method, it is necessary to know the conductivity of wash water, feed and tail streams, as well as performing some calibration tests to evaluate the two constants of the linear relation between bias and the volumetric fraction of wash-water under the interface. This method has shown good results in laboratory tests with two-phase systems (salty water and air). In these cases, the bias rate (for calibration purposes) was independently evaluated through a water balance. For estimating bias rate in a three-phase system, the knowledge of some other variables like the percentage of solids of the slurry and the percentage of solids of the froth is required.

### 1.2.3 Gas dispersion variables

Gomez and Finch [25] have reported that "gas dispersion is the collective term for superficial gas (air) velocity (volumetric air flow rate per unit cross sectional area of cell), gas hold-up (volumetric fraction of gas in a gas-slurry mixture), bubble size distribution, and bubble surface area flux". Gas dispersion properties are directly related to the performance of the flotation process [30].

#### Superficial gas velocity

Superficial gas velocity ($J_g$) is ratio of the volumetric gas flowrate to the cross-sectional area of the flotation machine. It is proportional to the air addition rate and can be calculated as

$$J_g = \frac{Q_g}{A_{cell}} \tag{1.1}$$

where $Q_g$ is the volumetric gas flow rate and $A_{cell}$ is the cell cross-sectional area (Figure 1.2).

#### Gas hold-up

Gas hold-up represents the volumetric fraction of gas (or air) in a considered column zone (Figure 1.3). For practical uses, it is usually estimated somewhere in the collection zone. Gas

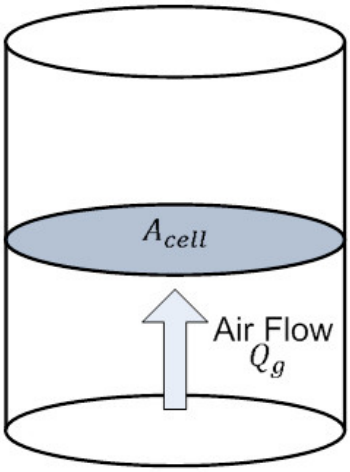


Figure 1.2: Superficial gas velocity

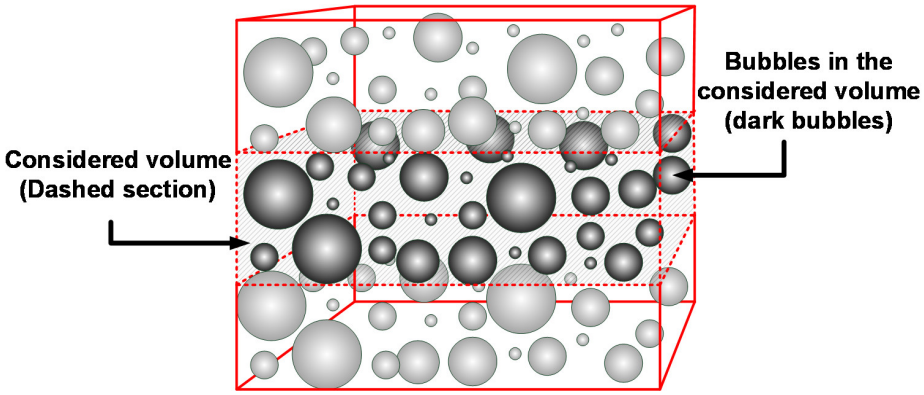


Figure 1.3: Gas hold up

hold-up strongly depends on the amount of air added, the frother concentration and the pulp viscosity, and the bubble size.

Gas hold-up can be measured directly by taking a sample of the slurry with bubbles and waiting until all the air reaches the top (displacement method). Other techniques uses a differential pressure based method, a conductivity measurement method based on Maxwells equation [84], sound tracking by using a SONARtrac device, among others.

### Bubble size distribution and bubble size

The bubble size distribution is a list of values (or a mathematical function) corresponding to the relative amount of bubbles present in the sample, sorted according size. Figure 1.4 shows two different distributions histogram and probability density function. Figure 1.4a is of easy calculation and usually used as quick reference, meanwhile the probability density function (Figure 1.4b) could be estimated by curve fitting algorithms/tools, but can give an accurate function to represent the probability distribution. In flotation columns bubble size depends on

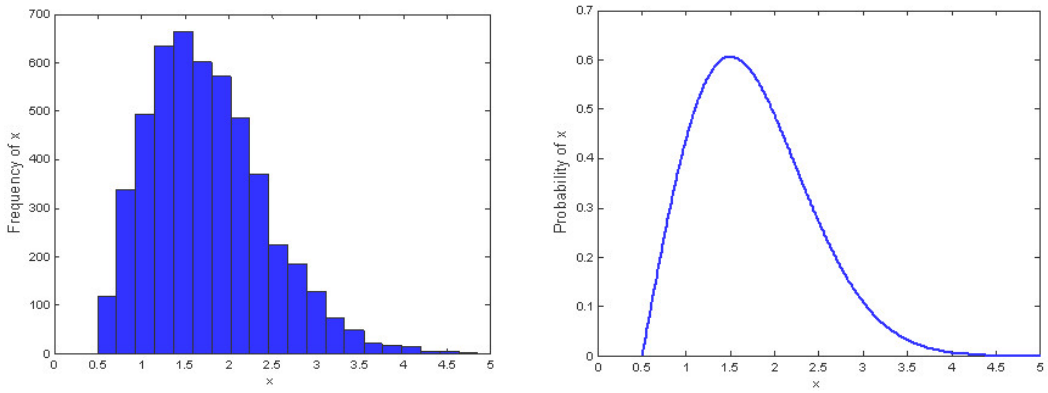


(a) Histogram

(b) Probability density function (PDF)

Figure 1.4: Different methods to represent bubble size distribution

the sparging device, solution chemistry (frother properties and concentration), pulp properties (i.e. density and viscosity) and, to a lesser degree, other factors as the pulp temperature or the pressure inside the column [79].

Instead using the bubble size distribution the mean bubble size is normally used since it is a scalar. This variable is considered to be one of the most important indicators of the gas dispersion efficiency. The bubble size is defined as the equivalent diameter of a spherical bubble. Usually the Sauter mean diameter (SMD or $D_{32}$) is used. It is defined as the diameter of a sphere that has the same volume/surface area ratio as the bubble of interest. It can be calculated as:

$$D_{32} = \frac{\sum_{i=1}^{n} d_i^3}{\sum_{i=1}^{n} d_i^2} \tag{1.2}$$

where $d_i$ is the i-observed bubble diameter and n is the total amount of measured bubbles. This method is often used in fluid problems given that it provides intrinsic data that help determining the mean bubble size. $D_{32}$ normally differs from the arithmetic mean (or $D_{10}$) which is calculated as

$$D_{10} = \frac{1}{n} \sum_{i=1}^{n} d_i \tag{1.3}$$

The Sauter mean diameter is equal to the arithmetic mean only when all the bubbles have the same diameter (standard deviation equal to zero). For all other cases $D_{32}$ is bigger than $D_{10}$.

### Bubble surface area flux

The bubble surface area flux ($S_b$) is defined as the amount of bubble surface area rising through a flotation column per cross sectional area per unit of time. That means that it depends on the bubble size and superficial gas velocity. Bubble surface area flux can be estimated for

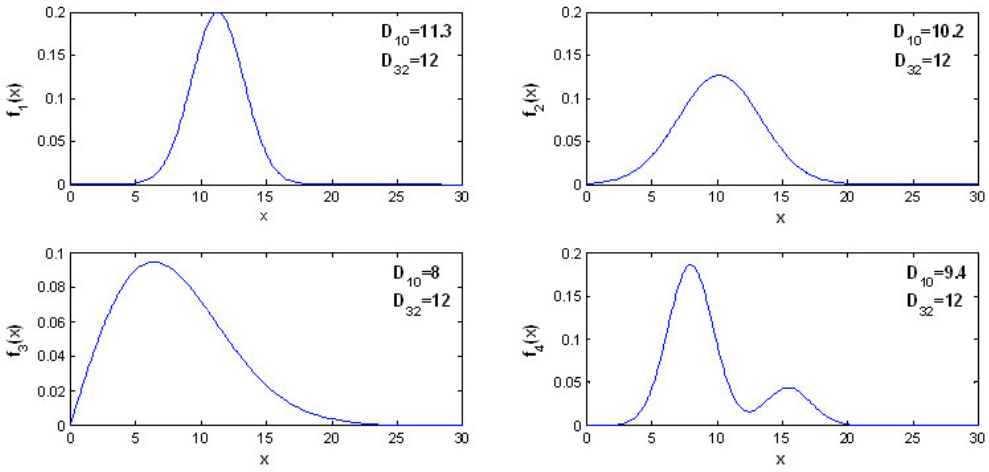


Figure 1.5: Four different distributions with the same $D_{32} = 12$

spherical bubbles as

$$S_b = \frac{6J_g}{D_{32}} \tag{1.4}$$

where $D_{32}$ is the Sauter mean diameter and $J_g$ is the superficial gas velocity.

The bubble surface area flux is used to describe the gas dispersion efficiency in flotation machines. The $S_b$ value is used to estimate the metallurgical performance as suggested by Gorain et al. [27], as well as Finch and Dobby [22] who propose that particle collection rate depends on the specific bubble surface.

## 1.3 Problem statement

Gas dispersion properties partially define the hydrodynamic conditions which govern the metallurgical performance of the flotation process. Current research is focused on these properties as a key to improve the valuable mineral recovery [2, 66, 63, 59]. Among these properties, the bubble surface area flux has shown the strongest correlation with the flotation rate [36].

The main problem of the estimation of the bubble surface area flux lies on the evaluation of the mean diameter of the bubbles. Different distributions could provide the same $D_{32}$ even if there are no bubbles having such a size; this is particularly the case of multimodal distributions. Industrial columns operate using multiple spargers to provide the required air flow rate which may lead to multimodal distributions. As a result, the estimation of $S_b$ could be an imprecise factor to determine the actual performance of the column. Figure 1.5 shows four different distributions with the same $D_{32}$ and different $D_{10}$.

Figure 1.6 shows the opposite case. A set of four different distributions with same $D_{10}$ and differents $D_{32}$. Notice that in both cases $D_{32}$ is bigger than $D_{10}$ and their values get closer as

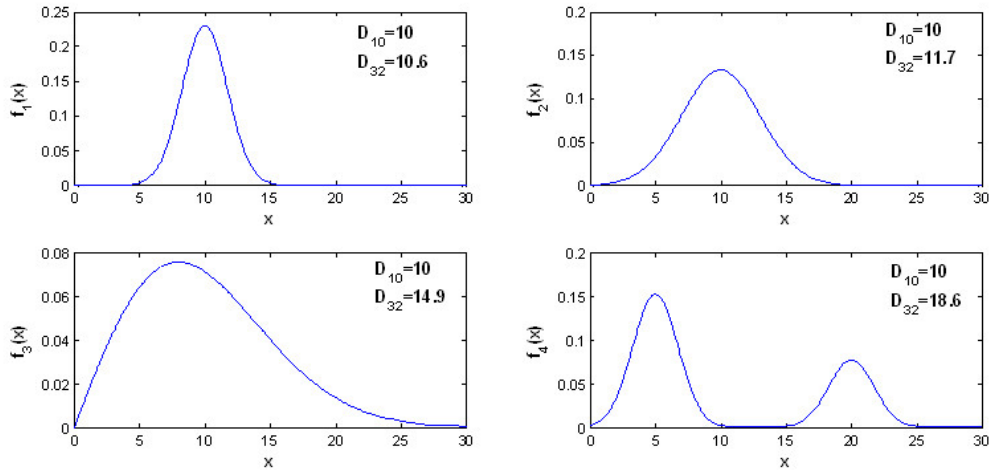


Figure 1.6: Four different distributions with the same $D_{10} = 10$

the distribution gets narrower.

In flotation processes, the bubble size is a probability density function which is dynamically related to the manipulation of the inputs of the process and the pulp properties. This output probability density function can dynamically change its moment and shape to another non-Gaussian distribution. Also, it can change from an uni-modal distribution to multi-modal and vice-versa. This introduces a new challenge given that traditional stochastic control methods do not support the requirements for this type of process.

It has been noticed that the current methods based on image processing for detecting and estimating BSD, only detects circular shapes [1]. This is an important issue since large bubbles are normally clustered with other bubbles of different sizes, thus not being accounted for, thus biasing the measurement of the total distribution.

Moreover, since the output distribution can change in different ways, is also necessary to find a dynamic representation to model the system. This model can be used for its observation and to analyze the controller design.

A final challenge is the ability of controlling such output distribution using multiple spargers. In this case, multi-modal distributions could be generated at the output of the stochastic system by independently manipulating the air flow and the shearing water flow for each sparger.

## 1.4 Research objectives

The main objective of this work is the development of a methodology for modeling and controlling the whole bubble size distribution rather than a scalar variable (the mean bubble diameter). This control strategy would be implemented to modify the BSD in a laboratory

flotation column, seeking ultimately a better match with the particle size distribution being processed.

Different methods have been proposed to model a probability density function, such as stochastic models, parametric decomposition and semi parametric decomposition [100, 40]. However, not all of these techniques support a mixture of distributions [91]. It is then be necessary to find an appropriate approach to model the dynamics of the bubble size distribution through changes in the system inputs (i.e. the shearing water and the air flow).

As a preliminary stage for the BSD sensoring, i.e. the image processing method used to determine the BSD, needs to be improved in order to increase the quality of the measurements. This step is important for a properly BSD modeling.

Once the modeling step will be completed, a strategy for controlling a bubble size distribution will be designed and tested in a laboratory flotation column working with a two-phase (water-air) system.

## 1.5 Contributions

The main contributions of this work are:

- To write an article for a new measuring conductivity device of dispersions on a flotation column. This article also includes the use of this new instrument to precisely determine flotation column variables, such as froth depth, gas hold-up and bias rate [78].
- To development a new method to measure BSDs, which greatly improves the existing ones. Part of this work was presented by the author at the World Mining Congress in 2013 [76].
- The conception of a dynamic model for BSDs using a parametric function (log-normal). Part of this work was presented at the 16th IFAC Symposium on Control, Optimization and Automation in Mining, Minerals and Metal Processing, in 2013 [77]. The redaction of this conference paper was done with the supervision of the co-authors.
- The design of a linear control strategy for BSDs generated by a single frit-and-sleeve sparger. Tests were carried out on a laboratory flotation column working with a two-phase (water-air) system. This chapter is currently being redacted by the author and the co-authors (Desbiens, A., del Villar, R. and Maldonado, M.) for submission to a journal paper.
- The participation in the redaction of five other articles as co-author,[57, 56, 58, 9, 10].
- The presentation of two conference papers: one as author [76], and another as co-author [9].

## 1.6 Outline

This document is organized as follows. **Chapter 2** describes the column set-up where the tests completed for the work mentioned in chapters 4, 5 and 6 were carried out. The actuators and sensors involved in this research work are also presented.

**Chapter 3** illustrates a new method developed for measuring the electrical conductivity in a flotation column to estimate three important process variables: froth depth, gas hold-up and bias rate. This new technique allows fast and accurate conductivity measurements in multiple points inside the column and at its ports (feed, tailings, wash water and concentrate pipes). This work was developed on an prior stage before the master degree by the author. However, the redaction of this article is part of the contributions of this thesis.

**Chapter 4** presents an image processing algorithm to accurately estimate the bubble size inside the flotation column. The size and number of bubbles in each image are evaluated by a bubble detection technique based on Circular Hough Transform (CHT). This technique allows overcoming issues related to the detection of large single bubbles as well as bubble clusters. Results were compared with manual (visual) counting, as well as a current method based on circular particle detection (CPD). Compared to the CPD algorithm, the CHT approach significantly improves the Sauter bubble diameter ($D_{32}$) estimation with a comparable processing time. This new technique is the base for the following sections.

**Chapter 5** uses the results of the previous chapter to identify a dynamic model for the BSD. The mean and standard deviation of a log-normal distribution are estimated by maximizing a likelihood function, leading to very good fits. A series of model identification tests were conducted by manipulating the gas flow rate and the shearing water flow rate setpoints of the used sparger. A Wiener model was then estimated to predict the corresponding mean and standard deviation of the log-normal distribution. Validation tests confirms the quality of the nonlinear model.

**Chapter 6** presents a Model-Based Predictive Controller (MPC) to control the BSD in the laboratory flotation column. The proposed approach leads to good control performances. This confirms the possibility to use this strategy to optimize the valuable mineral recovery by adequately selecting the BSD for a given particle size distribution.

The last chapter, **conclusions and future work**, summarizes the main conclusions of this thesis and suggests some guidelines for future work.

# Chapter 2

# Flotation column set-up

This chapter presents the flotation column set-up and its instrumentation used for the tests described in chapters 4, 5 and 6.

## 2.1 Column characteristics

A schematic representation of the experimental set-up is presented in Figure 2.1. The laboratory flotation column is made of 5.08cm diameter acrylic tubes for a total height of 7.2m. Feed is located at 5.1m from the bottom of the column. Tailings and concentrate streams are recirculated to a common tank containing the feed solution, i.e. tap water and F150, a frothing agent commonly employed in flotation to stabilize the froth. This solution is also employed as shearing water.

Data acquisition is performed by a HMI/SCADA software (iFIX®) working under Windows XP®operating system. An Opto 22I/O system centralizes sensor and actuator signals. The Opto 22I/O have a SnapB300-Modbus$^{TM}$ processor, analog input modules Snap-AIV 2Ch +/- 10V/5V DC and analog output modules Snap-AOV 0-10 V DC. They are installed in a main board SnapB16MC. The computer and the Opto 22 are connected by a RS-232 port and the communication protocol is based on Modbus$^{TM}$.

### 2.1.1 Frit-and-sleeve sparger

Air bubbles are generated with a stainless-steel frit-and-sleeve sparger located at the bottom of the column. The frit-and-sleeve sparger (Figure 2.2), consists of a porous cylinder surrounded by a sleeve forming a gap through which water is injected, shearing the air injected through the sparger into tiny bubbles [44]. This sparger allows the modification of the bubble size by manipulation of the shear-water flow rate through the gap. This means that bubble size can be varied independently of the used air flow rate. i.e. it provides an extra degree of freedom for controlling the bubble size distribution. The setpoint of the air flow rate loop ($J_G$) and

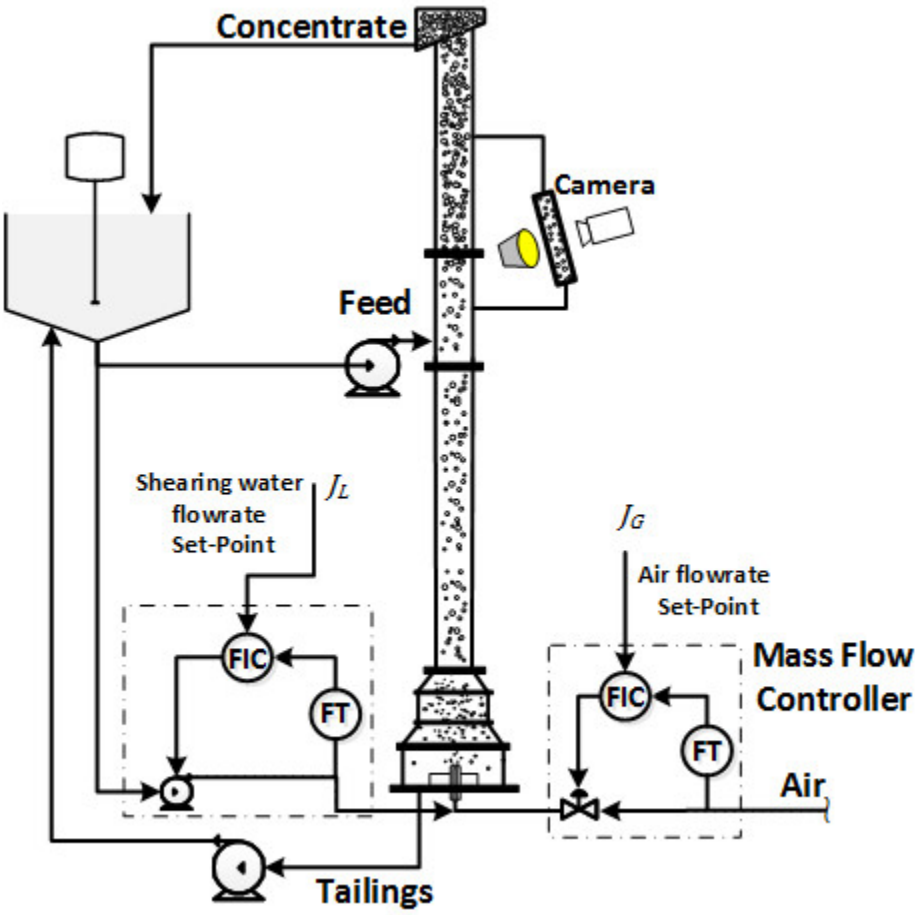


Figure 2.1: General laboratory column set-up

the shearing water ($J_L$) are the manipulated variables to control bubble size.

### 2.1.2 Bubble viewer

Bubble images are taken using a modified version of the McGill bubble viewer [25], connected to the column by a 1.27cm (0.5in) sampling tube (Figure 2.3) 20cm above the feed port. Bubbles are returned to the column after having been exposed in the viewing chamber and photographed with a computer controlled CCD camera model Sony DFW-X710. The viewing chamber is uniformly illuminated with a diffused LED white-light source, positioned opposite to the camera and aligned to this latter to have uniform and clear bubble contours, avoiding shaded areas. A computer running with Matlab© (R2013b) is programmed to take the pictures, analyze the images and estimate the log-normal PDF.

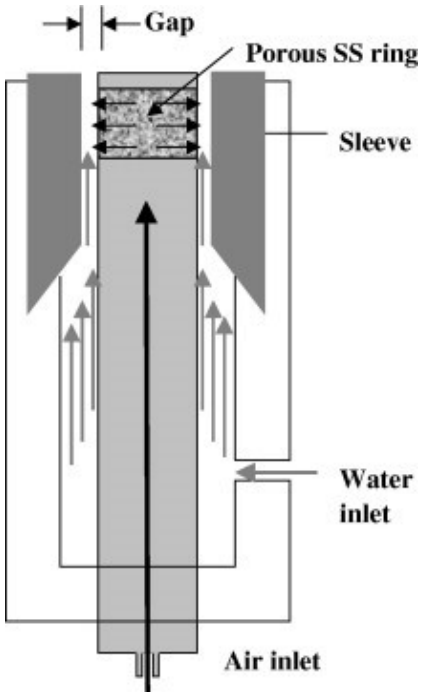


Figure 2.2: Frit and sleeve sparger prototype [44].

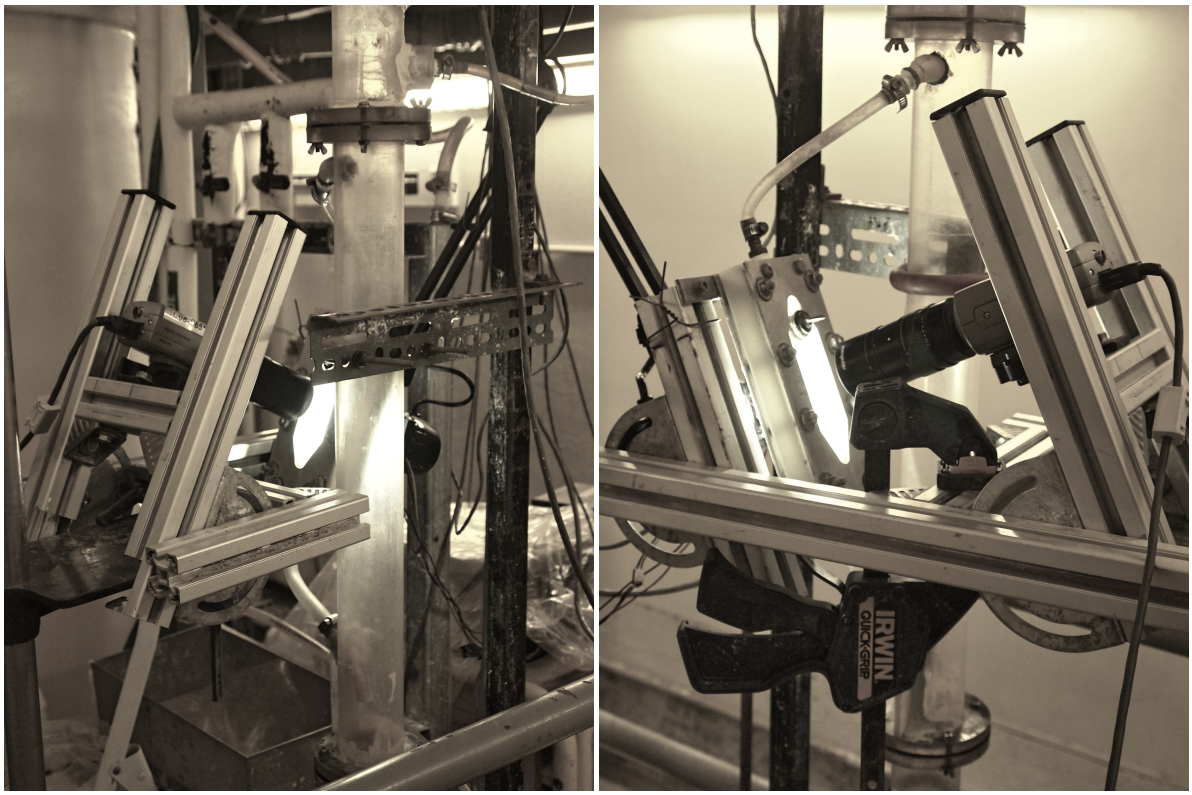


Figure 2.3: Bubble viewer

## 2.2 Column streams

### 2.2.1 Feed and tailing flows

Two variable-speed Masterflex$^{TM}$ peristaltic pumps (model 7585-30) are respectively used for injecting the feed at the middle of the column and for extracting the tailings at the bottom end. These pumps have a maximum capacity of 45 liters/min. Pumps speed is manipulated by two advanced variable-speed DC motor drive (Coleparmer$^{TM}$ model EW-70100-00). These drivers are connected to the Opto 22, and the pump speed is manipulated directly from iFIX$^{TM}$.

### 2.2.2 Shearing water flow rate

Shearing water is injected by a gear pump Enginegear (model GP-301). Its maximum capacity is 10 liters/min. One Cole-Parmer flow meter (model RK 32704-10) is employed to measure the shearing water flow-rate. This flow is regulated by manipulating the speed of the gear pump with a PID controller (Moore 353). This controller receives the setpoints and sends a signal of 4 to 20mA to the pump speed driver (Analog Servo Drive model 12A8 PWM). The communication is made by a RS-485 port.

### 2.2.3 Gas flow rate

The superficial gas flow rate is calculated from the measurement of the mass flow sensor/controller model Aalborg GFC17 by using equation 1.1. This superficial gas flow rate ($J_G^{ref}$) is at reference conditions (21.1°C and 1atm). Therefore, this measurement must be compensated to the process temperature and pressure, by the following equation:

$$J_G = J_G^{ref} \left( \frac{1033.23}{1033.23 + P} \right) \left( \frac{T + 273.15}{294.16} \right) \tag{2.1}$$

where $P$ is the absolute pressure measured in cm$H_2O$ by a two-wire pressure transmitter model Wika C-10 installed at the bottom of the column, $T$ is the temperature in degrees Celsius also measured at the bottom of the column by a temperature transmitter model RTD-NTP-72-E, and $J_G^{ref}$ is the reference flow rate measured by the mass flow controller.

# Chapter 3

# A device for measuring conductivity of dispersions[1]

**Abstract** A device to measure pulp electrical conductivity in an industrial environment has been developed. It is based on a variable oscillator circuit whose output period of oscillation is proportional to the sample conductivity. This circuit requires a single point for its calibration, which facilitates its use in an industrial environment. A Nexys2 FPGA (Field Programmable Gate Array) is used to measure the oscillation period, display the data on a LCD screen, communicate the information to a computer by RS-232 and manage the switching of sample probes for multiple measurements. Results have confirmed a linear relationship between frequency and resistance over a wide operational range; between 0.1 mS/cm and 10 mS/cm. Its application in an industrial flotation process in order to estimate froth depth and gas hold-up without prior calibration under certain conditions is also explained and validated.

**Résumé** Un dispositif pour mesurer la conductivité électrique d'une pulpe dans un environnement industriel a été développé. Il est basé sur un circuit oscillateur variable dont la période d'oscillation de sortie est proportionnelle à la conductivité de l'échantillon. Ce circuit requiert un seul point pour l'étalonnage, facilitant ainsi son utilisation dans un environnement industriel. Un Nexys2 FPGA (Field Programmable Gate Array) est utilisé pour mesurer la période d'oscillation, afficher les données sur un écran ACL, communiquer les informations à un ordinateur par RS-232 et pour gérer la commutation des sondes d'échantillonnage pour les mesures multiples. Les résultats ont confirmé une relation linéaire entre la fréquence et la résistance sur une large plage de fonctionnement entre 0,1 mS/cm et 10 mS/cm. Son application dans un procédé de flottation industrielle pour estimer la profondeur d'écume et le taux de rétention de gaz sans calibration préalable, sous certaines conditions, est également expliquée et validée.

[1] A. Riquelme, A. Desbiens, R. del Villar, and M. Maldonado. "A device for measuring conductivity of dispersions". Measurements, 59:49-55, 2014

## 3.1 Introduction

Electrical conductivity, an intensive material property, has been used extensively to monitor some important variables of mineral separation processes such as froth depth, gas hold-up and bias rate in flotation systems [84, 5] as well as the interface between the clarification-compression zones in thickening [96, 89].

Traditional procedures used to estimate electrical conductivity electrifies the probe with an alternating current at a frequency that is high enough to avoid electrolysis and polarization [6]. Circuits measuring conductivity can be categorized in three different groups: a) those finding equivalent impedance by manipulation of particular circuit components such as variable RC impedances, b) those finding a relationship between conductivity and voltage drop measured at certain points of the circuit, and c) those finding a relationship between the period of a signal generated from an oscillator circuit and conductivity.

For the equivalent-impedance methods, different approaches have been studied. Ferrara et al. [21] designed an A.C. bridge to find the complete model, including the cell (RC model). This approach is completely manual and restricted to conductivities under 1 mS/cm. Rehman et al. [75] proposed a system for calculating a sample conductivity by using a four-electrode probe to avoid polarization and D.C. parasite components. This strategy is also based on a bridge balance that is manually adjusted to find the equivalent resistance. Jones et al. [41] aimed at an automated bridge balance to determine an impedance similar to that of the sample. Samples are inserted into a cell, and the bridge is balanced automatically every two minutes with a commercial four-terminal pair impedance bridge. Another balance method, proposed by Mercer et al. [62], evaluated the sample resistance using a two-steps tuning of a circuit designed mainly with operational amplifiers. Approaches based on matching conductivity with electrical components are usually manual and only valid on a restricted range of conductivity. Their stand-alone operation is complex and requires special components such as automated A.C. bridges.

Methods determining conductivity based on one or more voltage measurements are the most widespread given their high automation possibility. These techniques relate conductivity to some voltage drops in a circuit and the sample conductivity. Some approaches are complex, such as that of Lario-Garcia et al. [45], who proposed a three by three equation system to estimate conductivity. Other approaches result in a nonlinear relationship requiring previous computation such as that of the quadratic relationships [106, 69, 11]. The last one also proposed an automated circuit to measure multiple cells probes to estimate a conductivity gradient in a flotation column. This design offers serial communication to a computer to calculate conductivity using nonlinear functions The main disadvantage of this method is the high load produced in the power supply when all cells are connected. Furthermore, the resolution is adjusted by correctly selecting a set of components. Other techniques also include

temperature-based conductivity compensation [73, 74], leading to more complex functions to estimate conductivity. Da Rocha et al. [17] designed a simplified method in which the electrical conductivity is proportional to a voltage drop in a point of the circuit, requiring a single-point calibration. This method also allows for the selection of the measurement range using a switch to increment the precision for low-conductivity values. They proposed an automated circuit to measure multiple cells probes to estimate a conductivity gradient in a flotation column. This design also offers communication by serial port to estimate conductivity in a computer using nonlinear calculations. The main disadvantage of this method is the high load produced in the power supply when all cells are connected. Furthermore, the resolution is adjusted by correctly selecting a set of components.

Techniques where conductivity is a function of a voltage measurement are sensitive to noise, and their resolution is restricted to the number of output bits of analog-to-digital converters. This last characteristic limits its stand-alone use when conductivity changes over a wide range. In addition, since the relationship between measured voltage and conductivity is usually nonlinear, the resolution is related to the changes in the function slope.

The third category consists of methods wherein the conductivity of the sample is a function of the frequency of a proposed oscillator circuit where the probe is connected. Rosenthal et al. [80] used an oscillator whose output frequency was proportional to the conductivity. Due to the difficulty in measuring the oscillator circuit signal period, the output signal of the oscillator was rectified and a relationship between the rectified voltage in the output and the conductivity in the cell was found. Another approach is based on oscillators where the conductivity is a non-linear function of the output frequency. For instance, Hawkins [35] found a square relationship between conductivity and the oscillation frequency in a modified band-pass filter. This circuit is designed to measure conductivities as low as 1 $\mu$S/cm. Another design based on a logic gate oscillator was introduced by Sahoo et al. [83]. The conductivity was found to be proportional to the square of the oscillation frequency. The system design includes communication by serial port and is valid for conductivity ranging from 0 to 1 mS/cm.

Strategies where the frequency is measured to estimate conductivity, minimize the problem of noise and D.C. components. Measurement resolution can also be improved by increasing clock frequency which is less expensive than increasing the resolution of the analog-to-digital converter. Furthermore, they allow data to be transmitted over long distances with no signal degradation since they handle digital signals.

An electronic device used to measure electric conductivity is presented here. It is based on a variable oscillator circuit where one of its resistances is replaced by the one to be measured, so that it has a linear relationship with the circuit oscillation period. The operating range can be easily adjusted by changing the value two components of the oscillator, allowing high flexibility in choosing the desired range and precision.

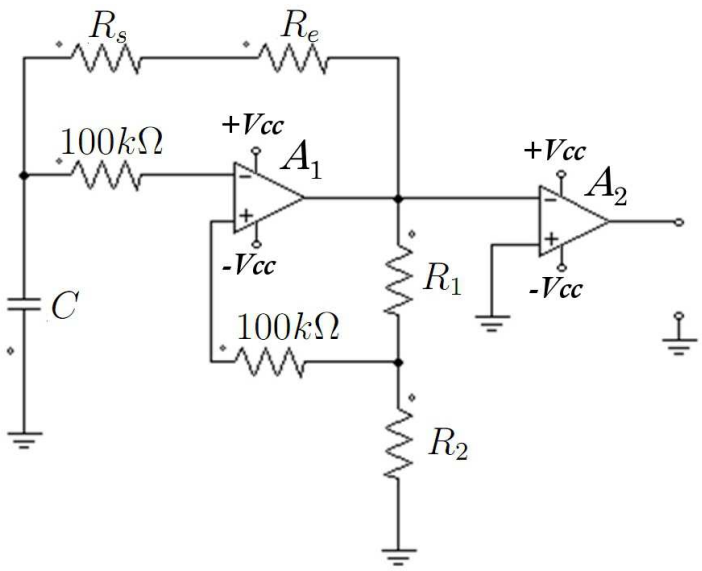


Figure 3.1: Square wave signal generator. *Re* is a variable resistance (e.g. the conductivity cell, see figure 3.2).

In addition, a system based on a FPGA is implemented to measure the oscillator period, display the data on a LCD screen, switch the probes for multiple measurements and send the measured data to a computer using serial communication for further analysis.

Its application for the calculation of some flotation variables (such as froth depth and gas hold-up) without requiring previous conductivity calibration is explained later.

## 3.2 Circuit description and principle of operation

The design of the proposed circuit is based on a simple square wave generator [29]. By generating a digital signal, it enables the transmission of signals over a long distance, it is less sensitive to noise than analog signals, it is easy to make corrections if the signal has been corrupted and the period measurement is simpler than for sinusoidal or triangular signals. Also, there is no need for an analog-to-digital converter to measure the signal thus simplifying the design of the circuit. Figure 3.1 shows the basic circuit, where $R_e$ is a variable resistance to be measured. Operational amplifier $A_1$ works as an oscillator and amplifier $A_2$ has a cut-saturation configuration to generate a full-range square signal. This stage converts the square wave into a digital signal. The oscillation period of the output signal $A_2$ is given by:

$$\tau = 2R_eC\ln\left(\frac{1+\beta}{1-\beta}\right) + 2R_sC\ln\left(\frac{1+\beta}{1-\beta}\right) = \alpha R_e + \tau_0 \tag{3.1}$$

where $\beta$ is given by

$$\beta = \frac{R_2}{R_1 + R_2} \tag{3.2}$$

Figure 3.2: Conductivity cell inside a pipe

Equation 3.1 is valid across the bandwidth of both operational amplifiers. As shown in equation 3.1, oscillation period $\tau$ is the result of two terms, one depending on $R_e$ (sample resistance) and the other on $R_s$ which is set to a fixed value. $R_e$ in Figure 3.1 is replaced by a conductivity cell made of two stainless steel electrodes (Figure 3.2). The resistance of a fluid contained in the cell is given by:

$$R_e = \frac{C_{CELL}}{k_e} \tag{3.3}$$

where $C_{CELL}$ is the cell constant whose value depends on the electrode area and section as well as the separation between electrodes; $k_e$ is the fluid conductivity to be measured. In this regard, it is possible to fully adjust a convenient range of the oscillation period for a known resistance variation. Using the value of capacitor $C$, the equation slope can be chosen. Through this design, the minimum and maximum periods are selected, so that the largest period is chosen to avoid polarization, while the minimum is related to the bandwidth of the oscillator. Furthermore, by selecting the value of resistance $R_s$ properly, the initial offset (Refer to section 3.5 for details). Parameter $\tau_0$ can be obtained by short-circuiting the conductivity cell and measuring the resulting oscillation period.

By combining equations 3.1 and 3.3, the following equation used to determine the electrical conductivity can be obtained:

$$k_e = \frac{\alpha C_{CELL}}{\tau - \tau_0} \tag{3.4}$$

This equation shows that a single-point calibration is enough to calculate the conductivity as a function of $\tau - \tau_0$.

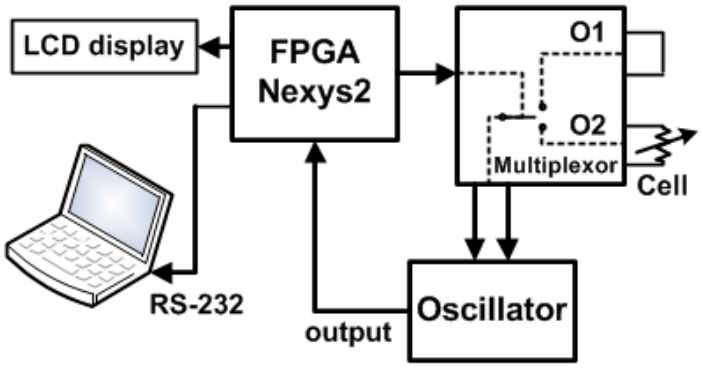


Figure 3.3: Block diagram of the measurement system

Figure 3.3 shows the setup of the measuring system. The multiplexor has two channels: O1 to measure the short-circuit period ($\tau_0$) and O2 to measure the desired resistance period ($\tau$). The oscillator range is chosen to be between 1 kHz and 10 kHz when the resistance in the channel O2 varies between 10 Ω and 1 kΩ. The resulting components are $R_1$=39 kΩ, $R_2$=47 kΩ, $R_s$=82 Ω and C=0.47 $\mu$F (Figure 3.1) all with 1 % tolerance. A $TL082CM$ chip provides both operational amplifiers required for the circuit. Amplifiers are powered with a dual supply of ± 5 V. Their bandwidth and slew rate are respectively 4 MHz and 13 V/$\mu$s. These specifications respect the required 9 kHz bandwidth (from 1 kHz to 10 kHz). Multiplexing is performed by photoMOS relays $AQY282EH$.

A FPGA Nexys2 card, manufactured by Digilent, was programmed to read the period from the oscillator circuit and manage the multiplexor by switching between output O1 (short-circuit) and O2 (Cell), to show the resulting periods on a LCD screen (PmodCLS from Digilent) and to send the results to the control computer using serial communication. Since the clock frequency of the FPGA is 50 MHz, the maximum frequency to be measured is set at 10 kHz. An de-bouncing block was implemented in the FPGA to avoid false-detection in the signal for frequencies over than 10.5 kHz that can be considered as noise. The minimum frequency is set at 1 kHz to avoid the polarization of the fluid whose conductivity is being measured. Figure 3.4 shows the signal at the output of the oscillator when the cells are switched between short-circuit (O1) and a 100 Ω resistance connected in O2. Short-circuit frequency is 10.09 kHz, while the output frequency when O2 is connected is 4.166 kHz.

## 3.3 Circuit performance

To test the circuit performance in terms of measuring resistance and conductivity, two scenarios were used. The first consisted in connecting a known resistance to channel O2 to test the linear relation between period and resistance. A resistance Ohm-Ranger having a range between zero and 4 MΩ in steps of 1 Ω and a precision of 1 % was connected to channel O2. Figure 3.5 shows the results obtained for $\tau_0$ and $\tau$. As described by equation 3.1, $\tau_0$ does not depend on

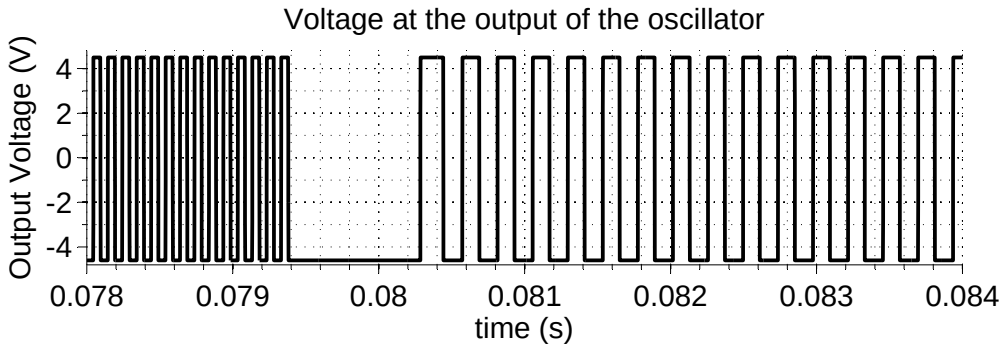


Figure 3.4: Signal at the output of the oscillator.

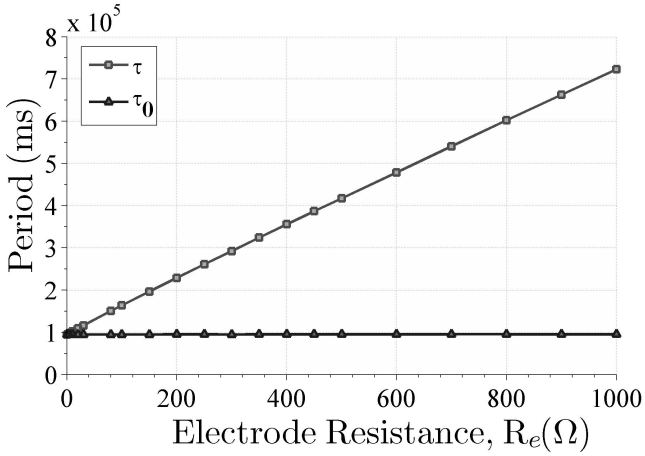


Figure 3.5: Plot of the experimental results using a variable resistance between 10 Ω and 1 kΩ.

resistance $R_e$ and period $\tau$ varies proportionally with $R_e$.

In a second scenario, a conductivity cell made of two stainless steel annular rings measuring 1 cm wide, 0.1 cm thick and 1 cm high (8 cm apart) was connected to amplifier O2. The oscillator circuit was then used to measure the conductivity of various solutions, each having different NaCl concentrations at 20 °C . Each solution concentration was measured in parallel with a laboratory conductivity-meter, model Oakton conductivity/TDS/C meter CON 11 Series, to have a reference measurement. The results obtained are shown in Figure 3.6, validating the linear relationship suggested by equation 3.4.

The preceding results confirm that the proposed conductivity meter only needs one calibration point. Thus, the circuit can easily be calibrated even if the components are not exactly known (1 % of tolerance in resistances and capacitor in this case). Following a calibration as explained in section 3.5, the performances of the instrument are summarized in table 3.1 [90]. The range where the sensor was validated is between 0 to 10000 $\mu$S/cm, with a minimum resolution of 5 $\mu$S/cm. Appendix A details the sensitivity analysis.

| Parameter | Value |
|---|---|
| Range | 0 to 10000 $\mu$S/cm |
| Accuracy | 5 % |
| Resolution | 0.5 % (5 $\mu$S/cm) |
| Nonlinearity factor (max) | 0.8 % |
| Repeatability | 35.5 $\mu$S/cm |
| Average residual error | 196 $\mu$S/cm |

Table 3.1: Calibration summary.

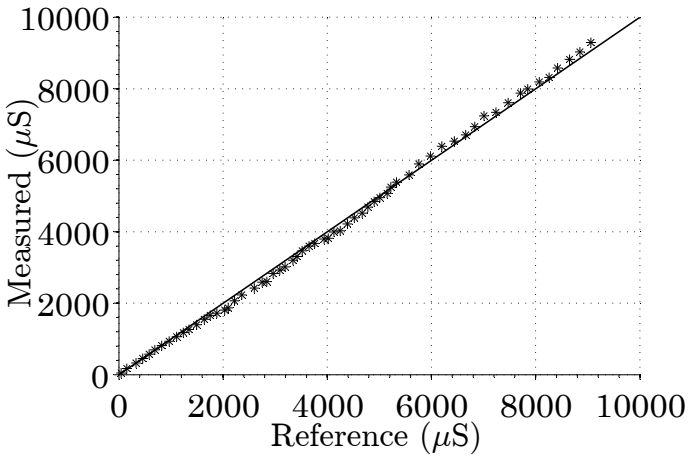


Figure 3.6: Conductivity of the experimental results obtained by changing the conductivity between 100 $\mu$S/cm and 9 $mS/cm$

These two experiments demonstrate that the system can accurately measure both pure resistances and ionic conductivities, on a wide range of values.

## 3.4 Application to a flotation process

Column flotation is a mineral processing method used to separate valuable minerals from useless minerals (gangue). The process consists of injecting air bubbles into a column vessel (typically 12 to 14 m height) where ground ore slurry is introduced at approximately 2 m from the top. Air is dispersed into bubbles at the bottom part of the column by using a device called "sparger". In order to provide the required air flow rate to an industrial column an array of several spargers is usually implemented. Prior to its introduction into the flotation column the slurry is conditioned with the proper chemicals that render the surface of valuable minerals hydrophobic so that it can attach to the rising bubbles. These bubble particles aggregates rise to the top of the column forming froth rich in valuable minerals. The flux of froth overflowing from the top of the cell is usually the valuable product, or concentrate. On the other hand, the gangue, which does not attach to the rising bubbles, leaves the column through its bottom part in a stream called tailings. Some process variables can be inferred from pulp conductivity

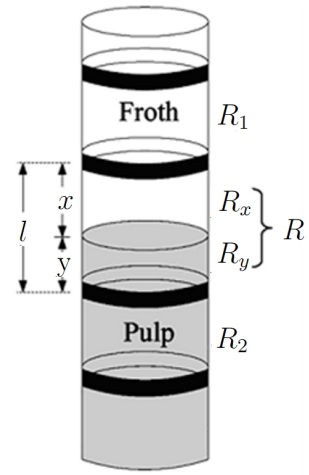


Figure 3.7: Configuration of the electrodes for level calculation.

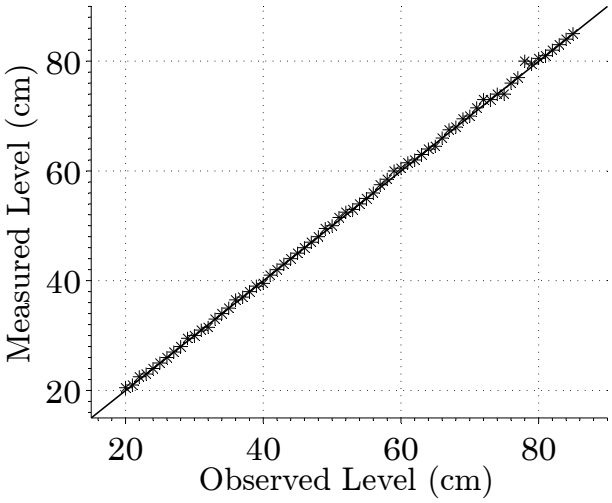


Figure 3.8: Validation of level estimation.

measurements. The next two sections rapidly describe how froth depth and gas hold-up can be estimated. More details on the froth depth estimation an its use for control purposes are found in [51, 95, 52, 9]. References [52, 9, 94] give more details on the estimation of gas hold-up and its application in control systems. Bias rate is another flotation column variable that can be estimated from conductivity measurements and thus controlled [52, 9, 55].

### 3.4.1 Froth depth estimation

This variable is estimated through the conductivity profile in the upper section of the column. Since the air content of the collection zone (bottom part of the column, Fig. 3.7) is quite different from that of the cleaning zone (upper most part of the column, Fig. 3.7), the position of the pulp-froth interface is assumed to be where the largest conductivity change exists

[95]. Gregoire [31] proposed a method to calculate the interface position within this cell as a function of the resistance measured over, below and in the cell where the froth-pulp interface is contained (Fig. 3.7). The fraction $x$ of the cell can be calculated as:

$$\frac{x}{l} = \frac{R - R_2}{R_1 - R_2} \tag{3.5}$$

where $l$ is the separation between adjacent electrodes. Finally, the relationship between resistance and conductivity is represented by:

$$k = \frac{C_{CELL}}{R} \tag{3.6}$$

where $C_{CELL}$ is the cell constant, similar for all cells if they have been properly built and installed in the column. Using equation 3.5 and assuming that the cell constant is the same for all pairs of electrodes, the fraction of cell containing the froth can be estimated by:

$$\frac{x}{l} = \frac{R - R_2}{R_1 - R_2} = \frac{\tau_R - \tau_{R_2}}{\tau_{R_1} - \tau_{R_2} - 2\tau_0} \tag{3.7}$$

Equation 3.7 clearly shows that no calibration is required to estimate the froth-pulp ratio in that particular cell.

This technique was improved by Maldonado et al. [51] keeping the main features of Gregoire's algorithm but improving the smoothness when the interface is near to an electrode or moving from one conductivity cell to another. This was done by considering the weighted average between the two possible values of froth depth determined by the first and second largest slope method proposed by Gregoire's algorithm.

A similar laboratory flotation column as the one of [51] was used for validation. Eleven stainless-steel conductivity electrodes in the uppermost section of the pilot flotation column aiming at the detection of the pulp-froth interface were installed. Figure 3.8 shows the validation of the method using this conductivity measurement circuit. Results shows a good correlation in the level detection with a maximum observed error of 0.5 cm.

### 3.4.2 Gas hold-up estimation

Gas hold-up is defined as the volumetric fraction of air bubbles inside a given volume of column. It can be used as a controlled variable to optimize the flotation process since mineral recovery strongly depends on the amount of bubble surface available.

Gas hold-up can be estimated using Maxwell's equation [60] as,

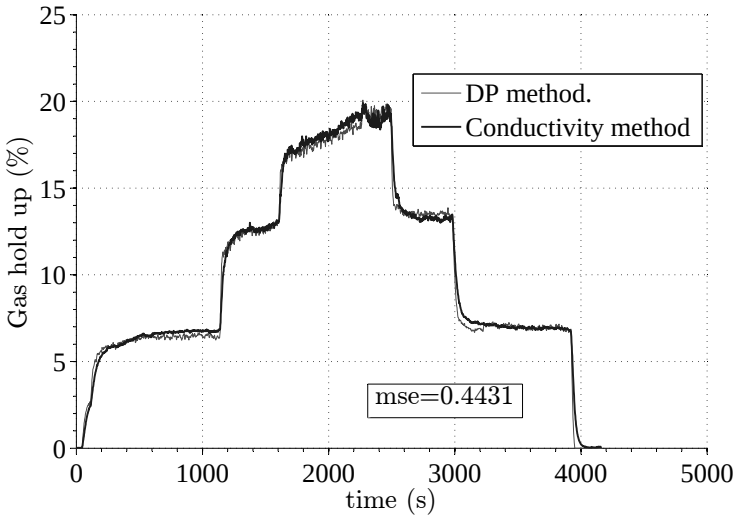


Figure 3.9: Validation of gas hold-up estimation.

$$\varepsilon_g = \frac{1 - (k_{slg}/k_{sl})}{1 + 0.5(k_{slg}/k_{sl})} \tag{3.8}$$

where, $\varepsilon_g$ is the gas volumetric hold-up, $k_{sl}$ is the conductivity of the pulp without gas ($sl$ for solid-liquid) and $k_{slg}$ is the conductivity of the solid-liquid-gas ($slg$) mixture. A sensor has been developed, based on two conductivity cells, one measuring $k_{slg}$ and the other specifically designed to avoid the presence of air bubbles [24]. Again, assuming the same cell constant to calculate conductivities $k_{sl}$ and $k_{slg}$, equation 3.8 could be modified using the measured periods of each sample ($\tau$) as follows:

$$\varepsilon_g = \frac{1 - \frac{R_{sl}}{R_{slg}} \frac{C_{CELL_{slg}}}{C_{CELL_{sl}}}}{1 + 0.5 \frac{R_{sl}}{R_{slg}} \frac{C_{CELL_{slg}}}{C_{CELL_{sl}}}} = \frac{\tau_{slg} - \tau_{sl}}{\tau_{slg} + 0.5\tau_{sl} - 1.5\tau_0} \tag{3.9}$$

Therefore, if the cell constants are the same for both cells, it is possible to estimate the gas hold-up directly using the calculated period instead of the actual conductivity. The set up of the column is similar as the one used for level validation adding the siphon and open cell as in [94]. To validate the results, the differential pressure transmitter (model ABB264DS) method was tapped between the cells to measure hold-up. For two phase system (air-water) this latter can be measured using the following relationship:

$$\varepsilon_g(\%) = 100 \frac{D_p}{H}, \tag{3.10}$$

where $D_p$ is the pressure differential in $cmH_2O$ and $H$ is the distance between taps (in this case 85 $cm$). Figure 3.9 shows that there is a good correlation between both measurement systems.

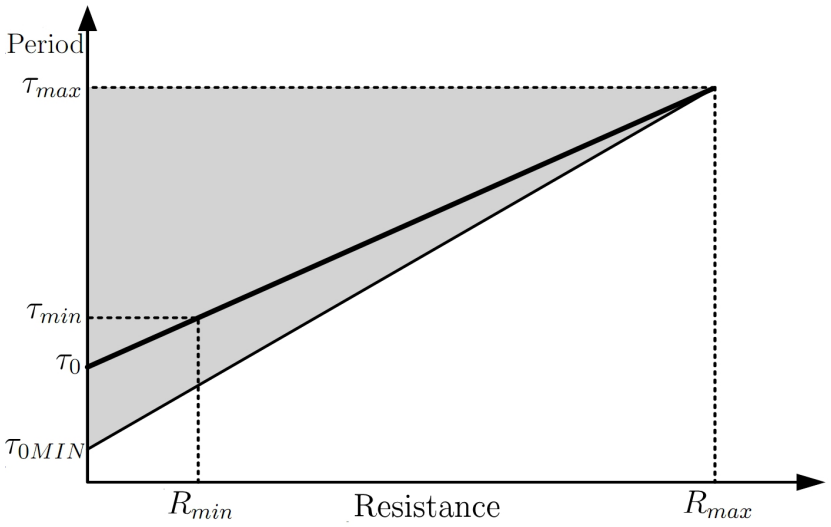


Figure 3.10: Operating zone for the oscillator. Gray zone shows the operational place. It is limited by $\tau_{0MIN}$ and $\tau_{max}$.

## 3.5 Calibration

To calibrate the sensor, the range of resistance in which the sample is going to vary for the foreseen conductivity range must be known. In this regard, the cell constant must be known to apply equation 3.3. This cell constant can be estimated using mathematical models or an empirical approach. This last approach consist in placing a standard solution in the cell, short-circuiting $R_s$ and modifying the value of $C$ until the circuit oscillates in a desired range (in terms of the characteristics of the operational amplifier); the cell is then replaced by a potentiometer that is adjusted to obtain the same oscillation period. Thus, the cell constant can be estimated using equation 3.3. With the value of the cell constant and regarding the desired range of conductivity, the maximum and minimum electrode resistance ($R_{min}$ and $R_{max}$) can also be calculated using equation 3.3. Once this range has been calculated, the following steps are suggested to calculate values $R_s$ and $C$:

1. Starting with $R_{max}$ (minimum conductivity value), it is possible to assume that this resistance is much larger than $R_s$ and so equation 3.1 can be approximated to:

$$\tau_{max} \approx 2R_{max}C \ln \frac{1+\beta}{1-\beta} \tag{3.11}$$

   where the only unknown is $C$. $\tau_{max}$ is the maximum desired period of 1 ms. Once $C$ has been calculated, the period obtained can be checked using a potentiometer with the value of $R_{max}$.

2. $R_s$ can then be evaluated by first setting the frequency range for the oscillator. The first constraint is to set a minimum period $\tau_{min}$ for the minimum value of resistance ($R_{min}$),

and the second aims to have a $\tau_0$ value greater than the bandwidth of operational amplifier $\tau_{0MIN}$; this last value depends on the properties of the operational amplifier. In this case, a maximum frequency of 20 kHz (0.05 ms) is suggested. The gray section in Figure 3.10 indicates the operating range. $R_s$ was chosen to have a certain $\tau_{min}$ within the constraint range. Consequently, $\tau_0$ is bigger than $\tau_{0MIN}$.

Some recommendations for the design of the cell must also be indicated. For the implementation of this measuring circuit, a maximum resistance of 80 kΩ in the cell is recommended. In such a case, the oscillator capacitor value will not be too small and the short-circuit period will not be too large, which implies that $R_s$ has a low value and that the approximation suggested in equation 3.11 is valid. The minimum resistance of the fluid cannot be too low either as it results from the use of solid-state relays and the resistance of wires and connections. A minimum resistance of 500 Ω is suggested to avoid problems in this regard. For an easy cell-constant adjustment without having to modify the ring electrodes, the distance between them should be changed.

## 3.6 Conclusions

A low-cost circuit used to measure resistances, and thus conductivities, has been presented. It is based on a square wave generator. The frequency of oscillation is proportional to the sample conductivity. This system can precisely measure a wide range of conductivities using a single-point calibration procedure. The measure of the oscillatory period is performed by a FPGA-based card. Its allows flexibility in the undertaking of various tasks simultaneously and its high-speed clock (50 MHz). As future work, other standard communication protocol can be implemented on the FPGA.

Although other period-measuring techniques can be used, (i.e. an oscilloscope or a micro controller) the proposed circuit is simpler, cheaper and more practical in an industrial environment. The design of the oscillators must respect certain constraints to enable the devices to operate within a proper precision range. It is critical to consider the bandwidth of the operational amplifier and the minimum frequency to avoid polarization of the measured fluid in a proper design. This new conductivity measuring system can be used to accurately estimate some flotation variables such as froth depth and gas hold-up with little or no calibration.

A convenient method for evaluating variables such as those mentioned above could allow for the optimization of the flotation process, e.g. increase the recovery of the valuable mineral to the concentrate while keeping an adequate value of the concentrate grade to maximizing the economic return.

The control of froth depth and gas hold-up of a flotation column using the proposed device is presented in [52, 9].

# Chapter 4

# Bubble detection in flotation columns based on Circular Hough Transform[1]

**Abstract** A bubble detection technique based on Circular Hough Transform (CHT) has been implemented for bubble size distribution (BSD) determination in two-phase (gas-liquid) systems. This technique allows overcoming issues related to the detection of large single bubbles as well as clusters. A high resolution CCD (charge-coupled device) camera is used to capture bubble images. The digital images are automatically pre-conditioned to eliminate the background, eventual noises, and to enhance the contrast. Tests were carried out in a laboratory flotation column using variable concentration of frother and air flow-rates. Results were compared against manual (visual) count, as well as a commonly used bubble detection method based on circular particle detection (CPD). The CHT-based technique allows proper detection and measurement of bubble clusters, large bubbles, and also incomplete bubbles in the image frame. Results obtained are very similar to those resulting from manual counts. Compared to CPD algorithms, the CHT approach significantly improves $D_{32}$ estimation (error of 3% instead of 18%) with a comparable processing time.

**Résumé** Une technique de détection de bulles basée sur la transformée circulaire de Hough (CHT) a été mise en place pour la détermination de la distribution de la taille des bulles (BSD) dans un système en deux phases (gaz-liquide). Cette technique permet de régler les problèmes liés à la détection de grosses bulles individuelles ainsi que des grappes de bulles. Une caméra à haute résolution est utilisée pour capturer des images de bulles. Les images numériques obtenues sont automatiquement pré-conditionnées pour éliminer le fond et les bruits éventuels tout en améliorant le contraste. Des essais ont été effectués dans une colonne de flottation de laboratoire en utilisant des concentrations différentes de l'agent moussant et des débits d'air. Les résultats ont été comparés à ceux du comptage manuel (visuel), ainsi qu'à un procédé de

[1] A. Riquelme, J. Bouchard, A. Desbiens and R. del Villar. "Bubble detection in flotation columns based on cicular Hough transform". World Mining Congress, 1:2-10, 2013

détection de bulles couramment utilisé basé sur la détection de particules circulaires (CPD). La technique basée sur la CHT permet la détection et la mesure des grappes de bulles, de grosses bulles et aussi de bulles incomplètes qui se trouvent dans le cadre de l'image. Les résultats obtenus sont très semblables à ceux obtenus par comptage manuel. Par rapport aux algorithmes de CPD, l'approche CHT améliore considérablement l'estimation du $D_{32}$ (erreur de 3% au lieu de 18%) avec un temps de traitement comparable.

## 4.1 Introduction

Gas dispersion properties play an important role in flotation as they partially determine the metallurgical performance. One of the most relevant variable is the bubble surface area flux ($S_b$), which is usually calculated as a function of the gas rate ($J_g$) and the Sauter bubble mean diameter ($D_{32}$) determined from the bubble size distribution (equation 1.4). The Sauter bubble diameter is defined as the diameter of a set of identical size bubbles having the same total surface and volume as the original BSD. After some simplifications, the following formula is obtained:

$$D_{32} = \frac{\sum_{i=1}^{n} d_i^3}{\sum_{i=1}^{n} d_i^2} \tag{4.1}$$

where $d_i$ is the i-observed bubble diameter and $n$ is the number of counted bubbles. $S_b$ actually represents the rate of bubble surface available for particle collection. On this regard, it is worth noting that Yianatos and Contreras [104] have developed a model for estimating the carrying capacity (maximum bubble coverage by particles) of a given flotation machine as a function, among some other variables, of the bubble Sauter mean diameter and $S_b$.

However, a given $D_{32}$ can be obtained with dissimilar shapes of bubble size distributions [55] (Figure 1.6), thus leading to multiple possible flotation recoveries. This is in accordance with the work done by Heiskanen [36] suggesting that matching the bubble size distribution with the particle size distribution of the valuable mineral would increase the recovery of this latter. The same concept also applies to the $S_b$, as a same value can be obtained from different $J_G$ and $D_{32}$ combinations. To control the entire BSD thus become essential to investigate the relationship between the flotation kinetics and hydrodynamic characteristics of the process. A proper measurement for BSD is required in order to design such a control strategy. Once this measurement is obtained, it would then be possible to estimate a dynamic model related to the manipulated variables available for control purposes.

Rodrigues and Rubio [79] reviewed different methods presently used to estimate the BSD, which include drift flux analysis, electro-resistivity, optical, and image analysis. These methods are also categorized as "intrusive" or "non-intrusive". Image analysis is probably nowadays the most widely used method for bubble size measurement, since it is the most straightforward

technique. However, it should be emphasized that vision-based techniques require a high processing computer capacity. Recent developments in digital image processing provide new opportunities for developing more specific and efficient algorithms to detect and measure bubbles in dispersions. Automated processing methods generally exhibit three distinct stages: filtering, edge detection and solid particle detection. Particle detection aims at identifying circular elements [34, 48, 108], thus excluding bubble clusters and large bubbles which are often non-spherical. Other methods include an off-line manual stage to take into account clustered and larger bubbles [97]), thus excluding possibilities of on-line process control applications.

The Hough transform (HT) is a frequently employed tool for detecting edges in images. It can isolate features of a particular shape within an image[20]. The calculation complexity of applying the HT is proportional to the number of parameters needed to describe the pattern [20]. The Circular Hough Transform (CHT) is a variation of the general HT, where the target shape is a circle. This transform is recognized as a robust technique for curve detection and it is widely used to detect overlapped circles [18, 28, 67]. Kjeldgaard [43] presents the detailed procedure. This method will be applied in this study, along with some image processing techniques, to properly estimate the BSD.

This strategy for bubble detection is proposed to address two issues: 1) the detection of non-perfectly circular bubbles, and 2) automation of the process. Tests were carried out in a two-phase laboratory flotation column (i.e. only water and air). Results are compared with those obtained using a circular particle detection algorithm and manual bubble counts. Section 4.2 explains the detection algorithm, i.e. the image preconditioning and the use of the circular Hough transform. Section 4.3 shows the experimental results and compares this new method with manual counting and the previous measurement system. Section 4.4 summarizes the main conclusions and describes the guidelines for future work.

## 4.2 Bubble detection algorithm

This section presents the fundamentals of an image processing application for bubble detection based on the CHT. The images used are 800 × 600 grayscale pictures. It is assumed that bubble sizes range between 5 and 80 pixels in diameter. Figure 4.1 shows a "raw" sample image which should undergo a series of preconditioning steps before applying the CHT; i.e. filtering, background subtraction, contrast enhancement and image inversion. All the steps were implemented in Matlab R2010a. Figure 4.2a shows a portion of the sample image to highlight the details of the image processing steps.

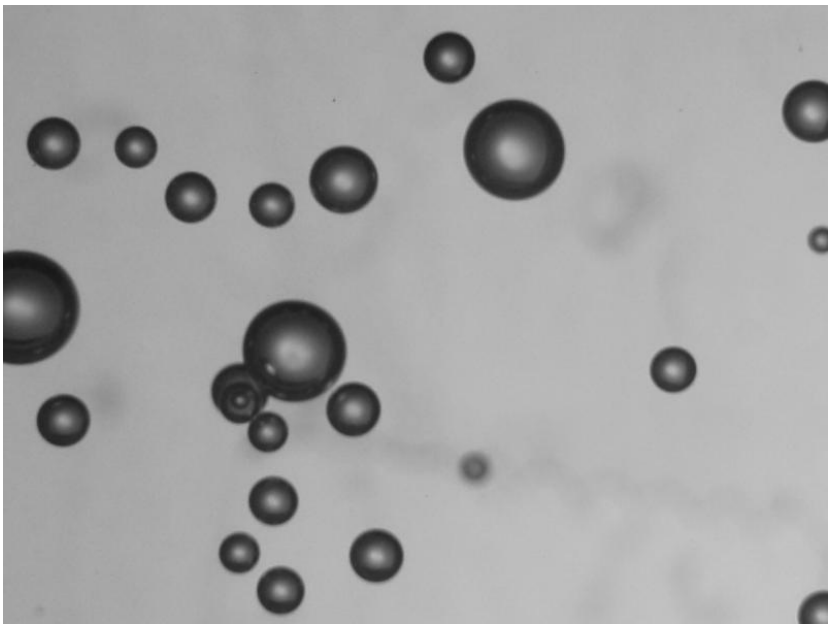

Figure 4.1: Sample image

### 4.2.1 Image preconditioning

#### Median filter

The first stage of the process consists in applying a 10x10 median filter [82]. This filter is a non-linear operation very efficient to reduce "salt and pepper" noises and to preserve edges in particles. In the present case, the noise sources are light reflection on bubbles and small solid particles in the feed. Figure 4.2b shows the result of applying a median filter.

#### Background subtraction

This operation creates a new image by applying an erosion operator, followed by a dilatation using a zone of 5x5 pixel disk into the previously filtered image [82]. This step removes "snowflakes" having a radius less than five pixels. The resulting image is later subtracted from the previously obtained image. This step allows extracting the gradient of the background produced by light diffusion and imperfections. Figure 4.2c is the resulting image after elimination of the background.

#### Contrast enhancement

The goal of this stage is to enhance bubble contour lines. The contrast is improved by an adaptive histogram equalization step [82]. In addition, the process also highlights bright inner parts. This generates a circle in the center of each bubble, which must be later eliminated. Figure 4.2d is the resulting contrasted image.

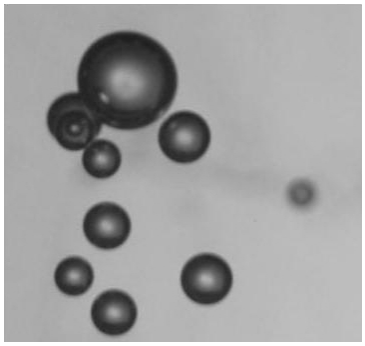

(a) Original image

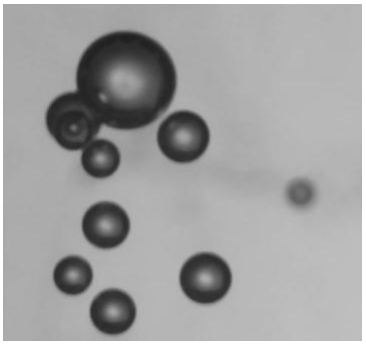

(b) Median filter

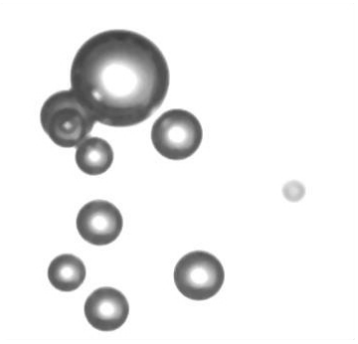

(c) Background substraction

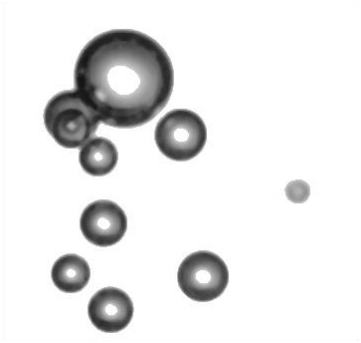

(d) Contrast tuning

(e) Inversion and filling

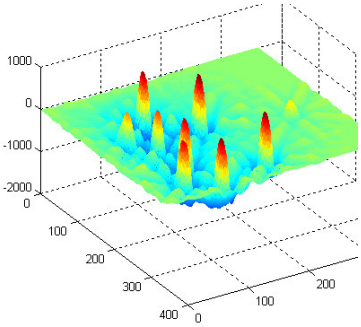


(f) Accumulation array

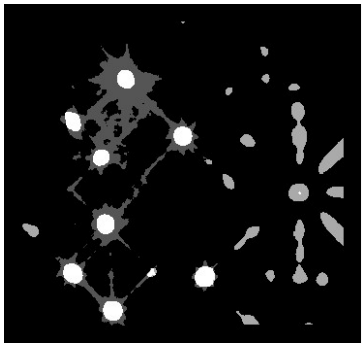

(g) Local maxima

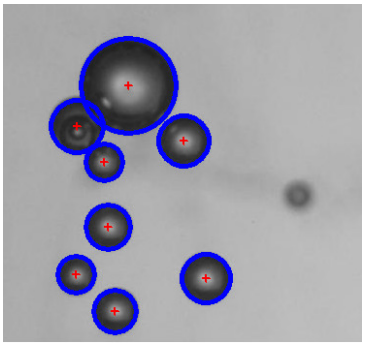

(h) Circle detection

Figure 4.2: Image analysis

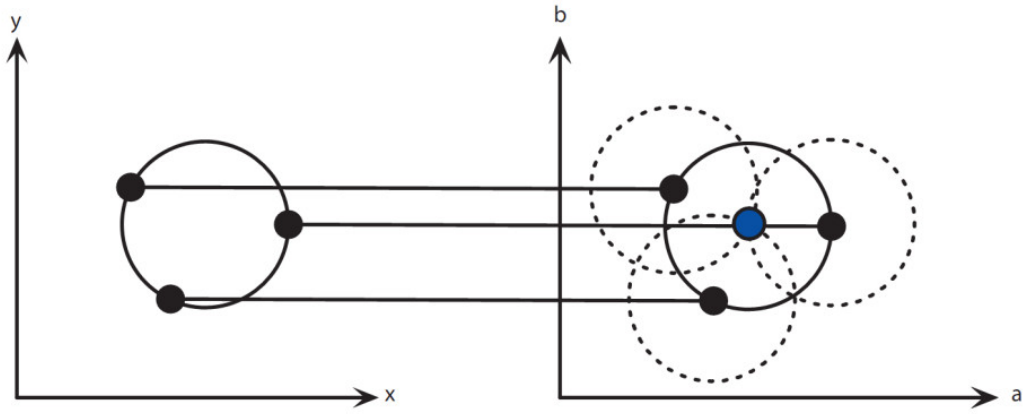


Figure 4.3: A circular Hough transform from the x, y-space (left) to the parameter space (right) for a constant radius (Kjeldgaard, [43]).

#### Filling holes

As explained above, a bright circle is produced in the center of each bubble as if they behave like a "mirror" reflecting the light source. This circle is filled with a gray surrounded tone before inverting the grayscale image. A hole is defined as a set of background pixels which cannot be reached by filling in the background from the edge of the image after applying a flood-fill operation [86]. Figure 4.2e shows the resulting image after filling the holes inside the circles.

### 4.2.2 Edge-map construction and Hough transform

Circular Hough Transform is a variation of the Hough transform aiming at detecting partially or completely circular shapes. The CHT transforms the edged image into a set of accumulated values in a parameter space. For each point of the edge, a circle with a target radius is drawn with the center in the point of interest. Figure 4.3 shows three points of a circle where the CHT is applied.

At the coordinates where the perimeter of each circle passes, the value of an accumulator matrix is incremented. It is straightforward to understand that local maximum of the accumulator is located at the center of each circle in the image. Figure 4.4 shows the result of the accumulators following the application of the CHT to a picture with two overlapping circles (Figure 4.4a). Values are accumulated in a matrix for all parameter combinations. After the process is completed, local maxima are searched in the accumulator array, indicating the presence of the center of a circle. Figures 4.4b and 4.4c show the maximum for each radius. The threshold for finding this maximum can be tuned to detect less perfect circles. As it was explained, the maxima of each accumulator are located in the center of the circle with the specific radius.

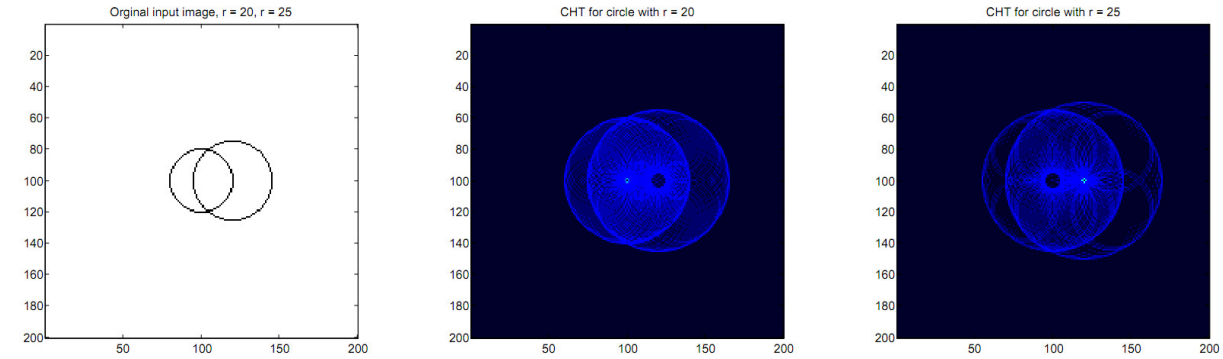


(a) The input image. (b) Hough transform where r = 20. (c) Hough transform where r = 25.

Figure 4.4: A circular Hough transform from the x, y-space (left) to the parameter space (right) for a constant radius (Kjeldgaard, [43]).

A modified version of the CHT, designed by [71], is based on the gradient field of an image to compute the accumulator. The maximum intensity in the accumulation matrix represents the center position of a sphere (Figure 4.2f). The detection of peaks in the accumulation array is done in three steps: 1) a Laplacian of Gaussian (LoG) filter to fill the transition between local peaks and to make easier the peaks separation, 2) a threshold to eliminate all the values which are not local maxima (Figure 4.2g, and 3) a region-growing algorithm to detect the centroid of the isolated region, to determine the center of each circle (Figure 4.2h). Detected circles are accumulated until the process is completed. The final results are the position and the radius of each detected circle.

## 4.3 Experimental results

Figure 4.5 shows the column configuration. Air flow rate setpoint ($J_G$) was manipulated to generate bubbles. Matlab© (R2013b) was used to control the camera trigger to take the samples and then to measure BSD by applying the designed algorithm. Refer to chapter 2 for more details regarding the column set-up.

Tests were carried out with different aeration conditions to generate a wide range of bubble sizes and shapes. Figure 4.6 shows two cases where most of the bubbles in the foreground are detected by applying the CHT-based method, irrespective of their size (including large ones), state of clustering, and completion (e.g. at the boarder of the frame). Bubbles in the background do not have a sharp enough boarder, thus they are not detected. Thus detection only applies for the first layer of bubbles in the viewing chamber. The processing time for each picture is around two seconds.

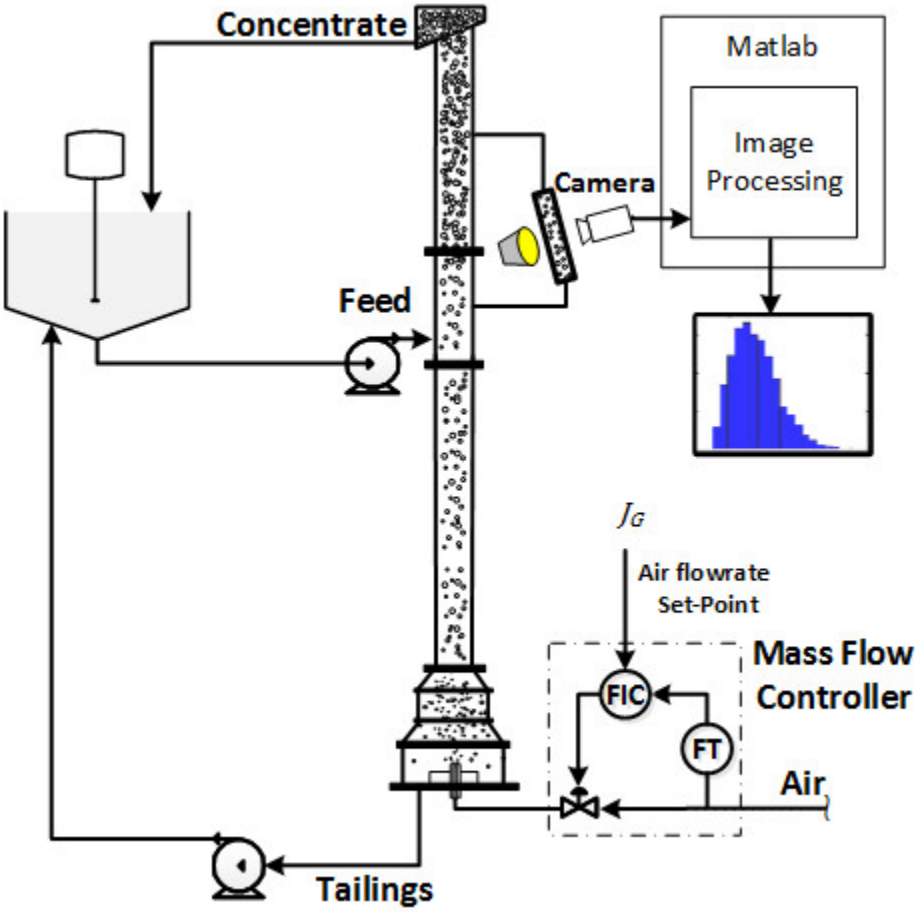


Figure 4.5: Laboratory column set-up

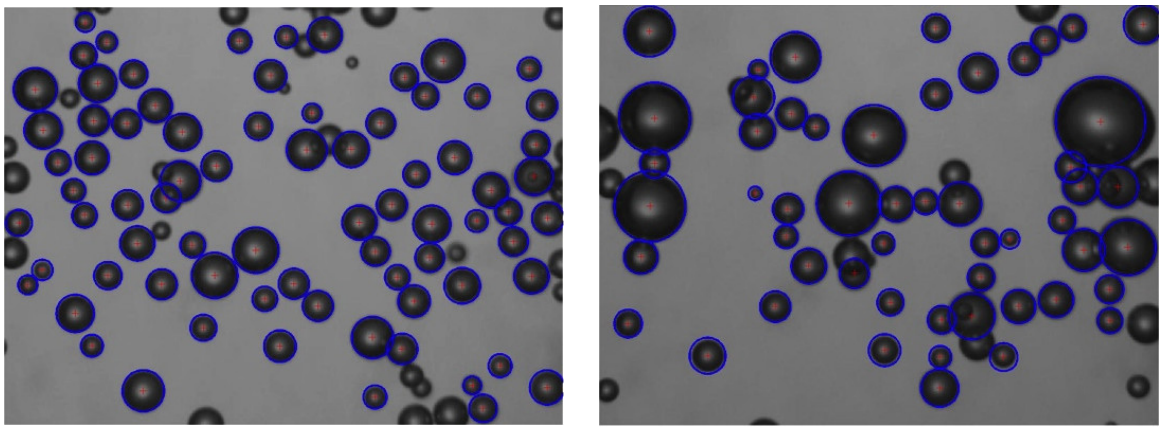

Figure 4.6: Examples of bubble detection results using the CHT

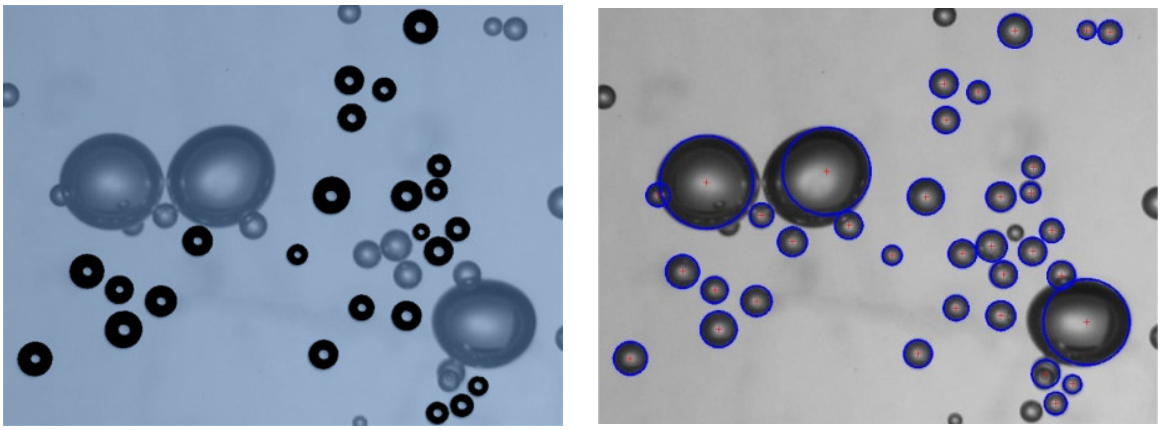

(a) Circular particle detection (b) CHT method

Figure 4.7: a) circular particle detection b) circular Hough algorithm

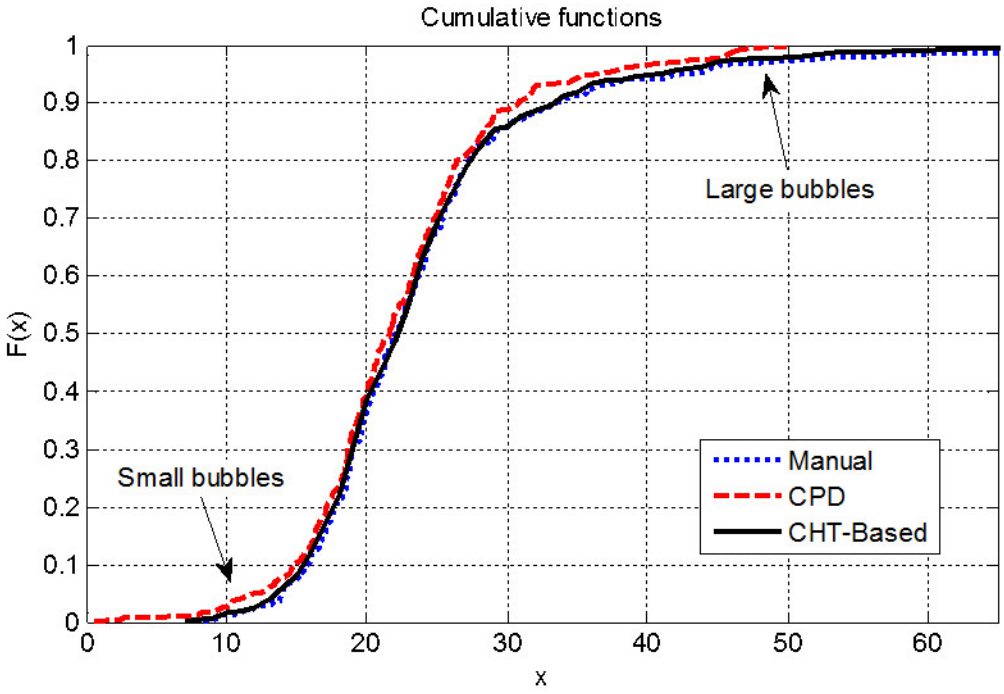


Figure 4.8: Cumulative functions comparison

### Comparison between different measuring methods

Three different methods for detecting bubbles were used: CHT-based, circular particle detection-based (ImageJ software), and a manual counting. Figure 4.7 compares the results obtained with (a) the circular shape method (black circles = detected, fuzzy ones = undetected) and (b) CHT-based method (detected bubbles are those with blue circles and a red cross marking their center). It quite evident that the CHT-based algorithm is highly superior in detecting clustered bubbles.

| Method | Bubble detected | $D_{32}$ (pixels) | $D_{32}$ error (%) |
|---|---|---|---|
| Manual | 537 | 33 | - |
| CHT | 525 | 32 | 3 |
| CPD | 377 | 27 | 18 |

Table 4.1: Comparison for the three method.

To compare the overall performance of the CHT-based algorithm, a set of 25 pictures was analyzed using the three methods mentioned above, and their cumulative function was estimated. Figure 4.8 shows the results. The cumulative function obtained with the CHT-based method is very similar to the obtained from manual counting. The performance of the algorithm based on circular particle detection decreases for bubbles larger than 30 pixels in diameter. For the reference manual counting, a total of 537 bubbles were identified. Table 4.1 summarizes the results for each method. Clearly, the CHT-based method is superior to the circular shape analysis algorithm, with a total number of detected bubbles comparable to the manual count. The average diameter ($D_{32}$) was also calculated, its value being more accurate for CHT-based method, with a relative error of 3% with respect to the manual counting.

## 4.4 Conclusions

A new application of the CHT for detecting bubbles in flotation columns was developed in this work. This method, based on the circular Hough transforms, allows the detection of all sorts of bubbles (clusters, imperfect circles, and bubbles at the borders of the frame). The CHT-based method leads to results consistent with a manual count, for the Sauter mean diameter, within a 3% error. The processing time is comparable to that of the commonly used circular shape based method. It must be emphasized that the CHT-based method requires automated pre-conditioning stages. A pre-tuning of the CHT algorithm is required to determine the threshold to find the local maxima of the cumulative function in order to detect less-circular shapes. Future work includes developing models and feedback control strategies for BSD in a laboratory flotation column.

# Chapter 5

# Bubble size distribution modeling in a flotation column[1]

**Abstract** Gas dispersion properties play an important role in flotation as they partially determine the metallurgical performance. The objective of this work is to obtain a dynamic model of the bubble size distribution in a two-phase (air and water) pilot flotation column. The steps are: 1) to measure and count the bubbles from digital images taken by a camera 2) to estimate a log-normal distribution of the bubble sizes 3) to estimate a Wiener model whose outputs are the mean and standard deviation of the distribution while the inputs are the gas and shearing water flow rate setpoints. The size and number of bubbles in each image are evaluated by a bubble detection technique based on Circular Hough Transform (CHT). This technique allows overcoming issues related to the detection of large single bubbles as well as clusters. Tests were carried out in the laboratory flotation column using different concentrations of frother and air flow rates. Results were compared with manual (visual) counting, as well as with a commonly used bubble detection method based on circular particle detection (CPD). The estimated number of bubbles is very similar to what is obtained with a manual (visual) count. Compared to a CPD algorithm, the CHT approach significantly improves $D_{32}$ estimation (error of 3% instead of 18% with the former) with a comparable processing time. Then, the mean and standard deviation of a log-normal distribution are estimated by maximizing a likelihood function thereby leading to very good fits for the distributions. Finally, a series of model identification tests were conducted by manipulating the gas flow rate setpoint and the setpoint of the shearing water flow rate through the sparger. A Wiener model was then estimated to predict the corresponding mean and standard deviation of the log-normal distribution. A validation test confirms the quality of the non-linear model.

[1] A. Riquelme, A. Desbiens, R. del Villar, and M. Maldonado. "Non-linear bubble size distribution modeling in a flotation column". This article is in process of submission to the International Journal of Mineral Processing.

**Résumé** Les propriétés de dispersion de gaz jouent un rôle important dans la flottation car elles déterminent partiellement les performances métallurgiques. L'objectif de ce travail est d'obtenir un modèle dynamique de la distribution de la taille des bulles dans une colonne pilote de flottation à deux phases (air et eau). Les étapes sont les suivantes: 1) mesurer et compter les bulles à partir d'images numériques prises par un appareil photo 2) estimer une distribution log-normale de la taille des bulles 3) estimer les paramètres d'un modèle Wiener dont les sorties sont la moyenne et l'écart type de la distribution tandis que les entrées sont la consigne de débit de gaz ainsi que la consigne du débit d'eau de cisaillement de bulles. La taille et le nombre de bulles dans chaque image sont évalués par une technique de détection de bulles basée sur la Transformée Circulaire Hough (CHT). Cette technique permet de surmonter les problèmes liés à la détection de grosses bulles individuelles ainsi que des grappes de bulles. Des essais ont été effectués dans la colonne de flottation de laboratoire en utilisant différentes concentrations de moussant et en variant le débit de l'air. Les résultats ont été comparés avec le comptage visuel, ainsi qu'avec un procédé de détection de bulles couramment utilisé qui se base sur la détection de particules circulaire (CPD). Le nombre estimé de bulles est très similaire à ce qui est obtenu avec un comptage manuel. Par rapport à un algorithme de CPD, l'approche CHT améliore significativement l'estimation de le $D_{32}$ (erreur de 3 % au lieu de 18 % avec l'ancien méthode) avec un temps de traitement comparable. Ensuite, la moyenne et l'écart type d'une distribution log-normale sont estimés en maximisant une fonction de vraisemblance, conduisant à de très bons ajustements pour les distributions. Enfin, une série de tests d'identification du modèle a été effectuée par la manipulation de la valeur de la consigne de débit de gaz ainsi que la consigne de débit d'eau de cisaillement de bulles. Ensuite, un modèle de Wiener a été estimé pour prédire l'écart moyen et standard correspondant de la distribution log-normale. Un test de validation confirme la qualité du modèle non linéaire.

## 5.1 Introduction

The BSD measurement in flotation process is essential to obtain a dynamic model aiming to control of the distribution. Density estimation deals with the problem of estimating the probability density function (PDF) of a set of data samples (bubble sizes in this case). The different existing methods for density estimation can be classified into three groups: 1) parametric methods, 2) non-parametric methods, and 3) semi-parametric methods.

Parametric methods are based on a defined and restricted function, leaving just a few parameters to be determined (depending on the objective function). The most common PDFs are Gaussian, exponential, Rayleigh and Chi-square. The estimation problem consists of finding the PDF model parameters such that the probability that the data have been generated by the resulting PDF is maximized (maximum likelihood). Since parametric PDF has a fixed function, a single function can fail to represent a distribution in some cases, e.g. for multi-modal distributions.

Non-parametric methods do not assume any fixed function, which allows modeling any data set without restrictions. So far, histograms have been used for quick visualization of the BSD [25]. The critical parameter in this particular case is the bin width. When it is very small, the resulting density model is spiky. On the other hand, when the bin width is too large, the resulting model is too smooth. In both cases, an inappropriate bin choice could not represent the distribution correctly [7]. One important feature for this method is that the estimated density exhibits some discontinuities. This is an important disadvantage for control purposes.

A semi-parametric method combines the advantages of both previous techniques and can comprise linear combinations of parametric functions. The parameters have to be estimated by some optimization technique. Maldonado et al. [55] proposed, for the bubble size density estimation, the use of a Gaussian Mixture Models (GMM) whose parameters are estimated based on an Expectation Maximization (EM) algorithm [91]. Maldonado et al. [52] proposed a control strategy formulated as an optimization problem which is based on GMM. However, the proposed cost function minimization algorithm does not guarantee a global minimum thereby suggesting the possibility to analyze other methods, i.e. free-derivative optimization algorithms such as genetic algorithms.

Previous works on flotation cells suggest that bubble size distributions can be reasonably well fitted with log-normal distributions [13, 30, 49]. In this work, log-normal functions are computed by the maximum likelihood estimation (MLE) method for BSD modeling purposes. This method will be explained in section 5.2.

Process dynamics can often be adequately modeled with linear time invariant system around an operating point. However, this strategy have limitations in describing highly non-linear processes. The computational complexity of modeling non-linear processes can be reduced by using some specific model structures. Particularly, some non-linear models are composed of linear dynamic subsystem and memoryless non-linear functions such as Wiener systems [70, 38, 26, 85], Hammerstein systems [88, 26], and their variations [68]. Other non-linear approaches for non-linear systems can be found in various articles [32, 65]. A Wiener model is a convenient technique for representing any time-invariant system with fading memory [8]. Specifically it is a simple choice for a multi-input multi-output (MIMO) system where the non-linear element depends on more than one output variable of the linear element. Given the characteristics observed in the BSD parameters dynamic of the estimated log-normal functions, a Wiener structure is a good approach to model this type of system.

This work uses the measurement technique explained in the previous chapter in order to measure BSD in a laboratory flotation column. A series of tests are carried out to analyze the behavior of bubble size. The obtained data is employed to model the BSD by a parametric method (log-normal distribution). Then the parameters of a non-linear Wiener process are

estimated to model the dynamics of BSD. Section 5.2 describes the process for estimating a parametric representation for the BSD. In section 5.3, the Wiener model identification steps are described. Finally, section 5.4 shows the experimental results for bubble size measurement, the BSD parametrization and the results after a Wiener model identification.

## 5.2 BSD parametrization

Previous researchers have suggested that bubble size distributions in flotation cells can be reasonably well fit with log-normal distributions [13, 30, 49]. A log-normal probability density function is defined as

$$P(x, x > 0) = \frac{1}{x\sigma\sqrt{2\pi}} exp\left[-\left(\ln\left[x - \mu\right]\right)^2 / (2\sigma^2)\right] \tag{5.1}$$

where $\sigma$ is the standard deviation and $\mu$ is the mean. The Sauter mean diameter, $D_{32}$ can be calculated from the log-normal distribution using directly the first and second moments of the function as [97]

$$D_{32} = exp(\mu + 5/2\sigma^2) \tag{5.2}$$

The maximum likelihood estimation (MLE) method was used to estimate the log-normal distribution best fitting the measured BSD [19]. The MLE aims at finding the values of the log-normal distribution parameters (mean and variance) which makes the modeled data most likely (maximizing the likelihood function).

Let's define a set of $N$ independent observations $x_n$, $(x_n \in X)$, coming from a distribution with an unknown PDF $f(x, \theta)$, where $\theta$ is the vector of parameters ($\sigma^2$ and $\mu$). The likelihood function is defined as

$$L\left(\theta \mid X_1, \ldots, X_n\right) = \prod_{i=1}^{N} f\left(x_i \mid \theta\right) \tag{5.3}$$

This estimation is the fundamental likelihood for a Gaussian distribution. To estimate a log-normal distribution, the following transform is made:

$$L_L\left(\theta \mid X_1, \ldots, X_n\right) = \prod_{i=1}^{N} \left[(1/x_i) f\left(\ln(x_i) \mid \theta\right)\right] \tag{5.4}$$

It is mathematically convenient to work with the logarithm of the likelihood function, called the log-likelihood. Since this is a monotone function, it does not modify the optimal solution. The log-likelihood is defined as

$$\ln\left(L_L\left(\theta \mid X_1, \ldots, X_n\right)\right) = -\sum_{l=1}^{N} \ln X_l + \sum_{l=1}^{N} \left[f\left(\ln(x_i) \mid \theta\right)\right] \tag{5.5}$$

The estimation of the expected log-likelihood of a single observation in the model is:

$$\widehat{l}_L = (1/n) \ln L_L \tag{5.6}$$

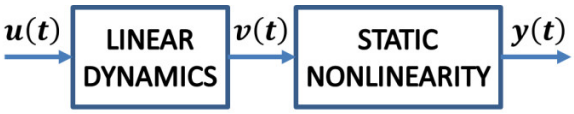


Figure 5.1: Wiener model structure

The standard approach to estimate the parameters of a defined PDF ($\theta$), is the MLE, which requires maximization of the following log-likelihood function.

$$\{\theta_{MLE}\} \subseteq \left\{ \underset{\theta \in \Theta}{argmax} \left[ \widehat{l}_L \left( \theta \mid x_1, \ldots, x_n \right) \right] \right\} \tag{5.7}$$

Taking derivatives with respect to $\mu$ and $\sigma^2$, and solving the resulting system of first order conditions, the MLE for the parameters are:

$$\widehat{\mu} = \left[ \sum_{i=1}^{N} \ln x_i \right] \Big/ N \tag{5.8}$$

and

$$\widehat{\sigma}^2 = \left[ \sum_{i=1}^{N} \ln (x_i - \widehat{\mu})^2 \right] \Big/ N \tag{5.9}$$

## 5.3 BSD Dynamic modeling

Developing an accurate model is a fundamental step toward the design of a successful control strategy. There are many non-linear models available for modeling of non-linear processes among which the Wiener model is one of the simplest non-linear representations. It consists of a linear time-invariant (LTI) dynamic system with a unitary gain in series with a static non-linear (memory-less) element (Figure 5.1). Usually the non-linear element is selected as an invertible function for control design purposes.

Many techniques have been suggested to identify Wiener models. Iqbal and Aziz [38] compares different methods such as the blind approach [3], the frequency domain approach [4], the support vector approach [92] and the maximum-likelihood approach [33]. In all these cases, the identification of a Wiener model is performed through three different methods [12]:

- *Simultaneous approach*. In this case, both elements are estimated at the same time,
- *Linear-Non-linear approach* (L-N). The parameters of the linear transfer function are first identified, and then this data is used to generate an intermediate signal to calculate the non-linear static element. For so doing, the non-linear element must be invertible.
- *Non-linear-Linear approach* (N-L): Here, the static non-linear parameters are first identified from the steady-state data; then the linear dynamic parameters are obtained from dynamic data. This last approach will be further described as it will be selected for process identification.

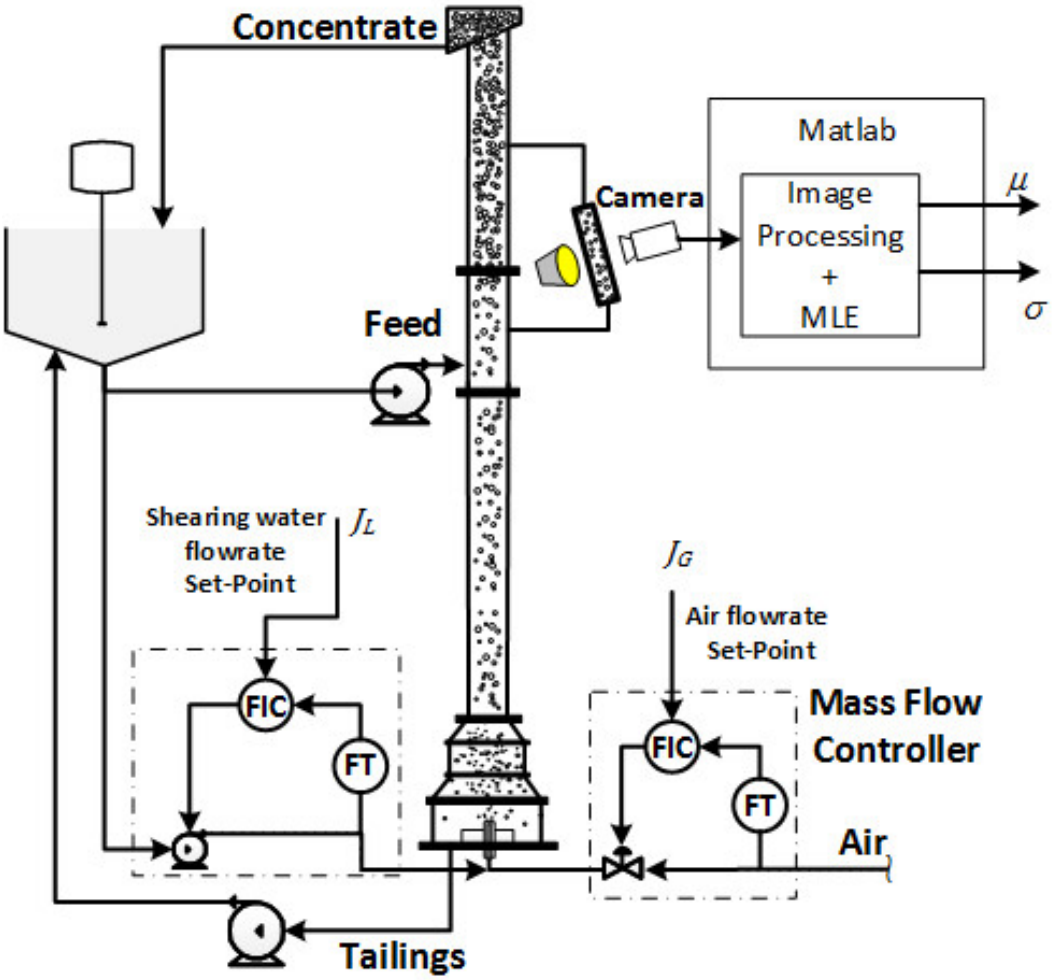


Figure 5.2: Laboratory column set-up

For the N-L approach, the steps for identification are the following:

1. Collect a set of steady-state data. Assuming that the linear element has a gain equal to 1, the static non-linearity can be identified from this set of data. This non-linear function must be invertible for the subsequent estimation of $v(t)$ (Figure 5.1).

2. Collect a set of dynamic data. Once the non-linearity has been identified and assuming that the non-linear function is invertible, it is possible to calculate $v(t)$ (Figure 5.1) by applying the inverse of the non-linearity. Then, the linear block can be identified using the data between $u(t)$ and $v(t)$.

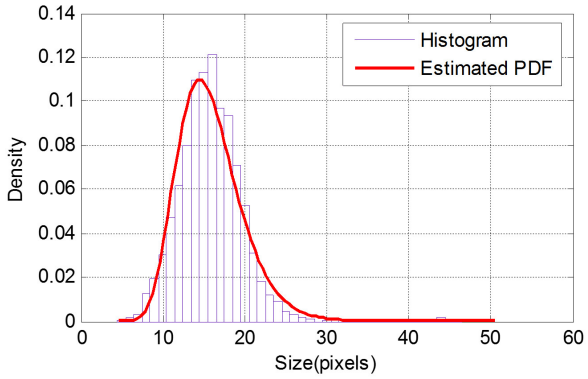


Figure 5.3: Histogram of BSD contrasted with the log-normal distribution.

## 5.4 Experimental results

Figure 5.2 shows the column configuration. In this case, BSD was modified by the manipulation of the air flow rate ($J_G$) and shearing water flow rate ($J_G$) setpoints. Chapter 2 explains the column set-up. Matlab© (R2013b) is used to control the camera trigger, to measure the bubbles size by applying the algorithm explained in chapter 4 and to estimate the log-normal PDF parameters.

### 5.4.1 Parametrization of bubble size distribution

Three types of test were carried out to validate the performance of the BSD parameterization. The first test was done to validate the obtained log-normal function with the computed histogram of the resulting measurements as proposed in the literature [13, 30, 49]. For the second type of tests, the air flow rate was varied while keeping the frother concentration constant. Log-normal parameters were estimated and $D_{32}$ was computed for comparison purposes. For the third type of tests, the air flow rate was kept constant while the frother concentration was changed. $D_{32}$ and log-normal parameters were computed and compared for validation.

**Test 1.** A set of 50 pictures taken from tests using different frother concentration and air flow rate. Pictures were all taken under steady state conditions. The maximum likelihood estimation algorithm was used to estimate the log-normal function, for all the collected bubbles corresponding to 50 frames. Figure 5.3 super-imposes the calibrated function over the histogram for a test done with a solution containing 10 ppm of F150 and a superficial gas velocity of 0.4 cm/s. The histogram was computed with equal bins of 1 pixel width each.

**Test 2.** Different gas rates were injected into the column trough the sparger. Frother concentration was kept constant at 10 ppm for all tests. The methodology consisted in collecting 50 bubble pictures in steady-state operating conditions. Table 5.1 summarizes the experimental results, showing the total bubble count, the estimated $D_{32}$ (obtained using equation 5.2), the reference $D_{32}$ estimated with the histogram (raw data from CHT-based detection method), the

| $\mathbf{J_G}$ **(cm/s)** | **0.4** | **1** | **1.6** |
|---|---|---|---|
| Bubbles counted | 4242 | 3356 | 2785 |
| $D_{32}$ est.(pixels) | 17.84 | 21.42 | 25.19 |
| $D_{32}$ ref.(pixels) | 17.98 | 21.5 | 25.31 |
| $D_{32}$ error(%) | 0.8 | 0.4 | 0.5 |
| $\widehat{\mu}$ | 2.7334 | 2.9306 | 3.015 |
| $\widehat{\mu}$ std. dev | 0.003734 | 0.003991 | 0.005514 |
| $\widehat{\sigma}$ | 0.2432 | 0.2312 | 0.2910 |
| $\widehat{\sigma}$ std. dev | 0.002641 | 0.002823 | 0.003901 |

Table 5.1: Log-normal estimation (10ppm F150).

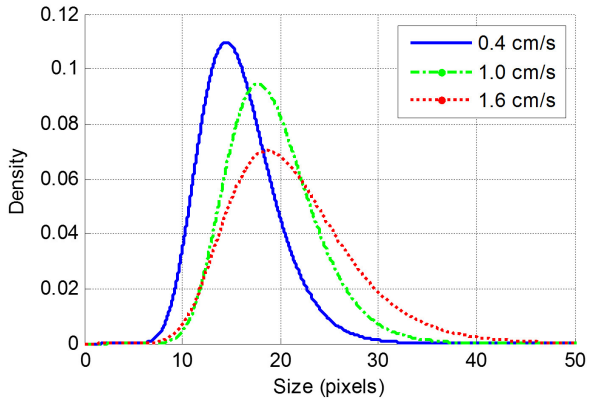


Figure 5.4: Log-normal estimations for different flow rates at the same frother concentration

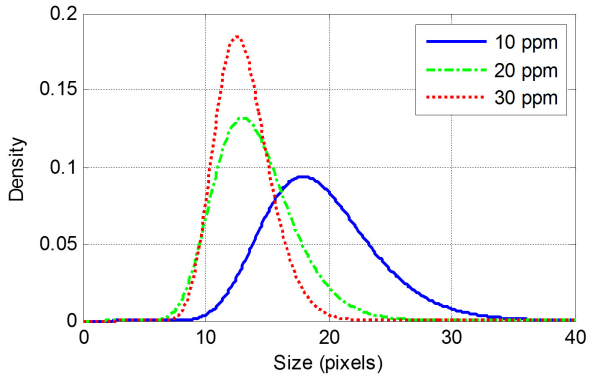


Figure 5.5: Log-normal estimations at the same flow rate for different frother concentrations

percentage of error with respect to the reference $D_{32}$, and the estimated log-normal function parameters $\mu$ and $\sigma$. It is quite evident that the error of the $D_{32}$ estimation is very low for all three cases. Figure 5.4 presents the estimated log-normal function for each of the three air flow rates at the same frother concentration.

**Test 3**. In these tests three different frother concentrations were used (10, 20 and 30 ppm), while keeping constant the superficial velocity of air (Jg=1 cm/s). Table 5.2 shows the results

| **F150 (ppm)** | **10** | **20** | **30** |
|---|---|---|---|
| Bubbles counted | 3356 | 7966 | 8700 |
| $D_{32}$ est.(pixels) | 21.42 | 15.55 | 13.84 |
| $D_{32}$ ref.(pixels) | 21.51 | 16.3 | 14.27 |
| $D_{32}$ error(%) | 0.4 | 4.6 | 3.0 |
| $\widehat{\mu}$ | 2.931 | 2.617 | 2.556 |
| $\widehat{\mu}$ std. dev | 0.003991 | 0.002529 | 0.001819 |
| $\widehat{\sigma}$ | 0.2312 | 0.2258 | 0.1697 |
| $\widehat{\sigma}$ std. dev | 0.002823 | 0.001788 | 0.001286 |

Table 5.2: Log-normal estimation ($J_G = 1cm/s$)

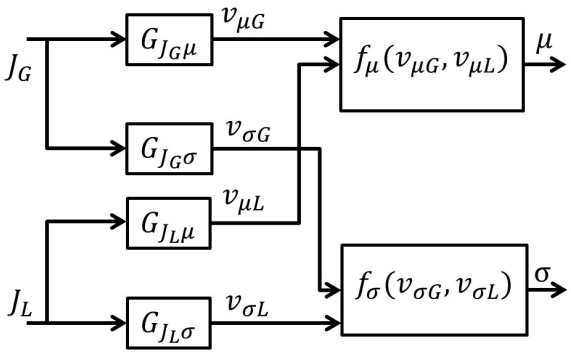


Figure 5.6: Wiener model structure

of the total bubble count, the estimated $D_{32}$ (obtained from equation 3), the reference $D_{32}$ calculated from the histogram (raw data from CHT-based detection method). $D_{32}$ is correctly estimated by the log-normal model. Figure 5.5 presents the three estimated log-normal functions. Not surprisingly, increasing frother concentration reduces the mean diameter and the distribution gets narrower.

### 5.4.2 Wiener process identification

Figure 5.6 shows the proposed model structure for the BSD. $J_G$ is superficial velocity of the gas (air) setpoint injected into trough the sparger, and $J_L$ is the superficial velocity setpoint of the shearing water. The outputs $\mu$ and $\sigma$ are the parameters that characterizes the log-normal function representing the bubble size distribution in the column. $G_{J_{G\mu}}$, $G_{J_{G\sigma}}$, $G_{J_{L\mu}}$ and $G_{J_{L\sigma}}$ are the transfer functions for each output and input combination, while $f_\mu(v_{\mu G}, v_{\mu L})$ and $f_\sigma(v_{\sigma G}, v_{\sigma L})$ represent the non-linear elements for each output.

In order to estimate a Wiener model, the N-L method is used. As described in section 5.3, the identification process is separated in two stages: determination of the non-linear element and then, estimation of the linear transfer functions having a unitary gain.

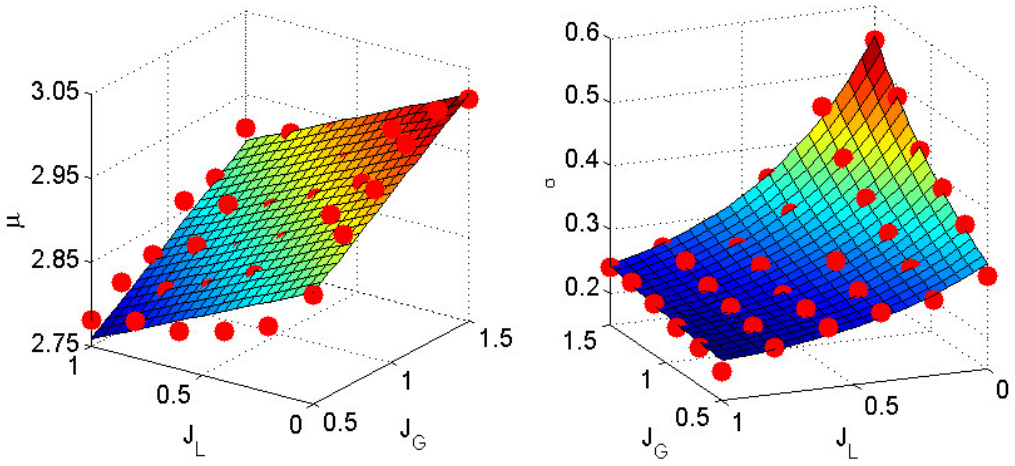


Figure 5.7: Surfaces estimation results. Left: $\mu$ estimation, right: $\sigma$ estimation

**BSD Static non-linearity**

In order to obtain the non-linear model, a set of data must be collected under steady-state conditions; later on a mathematical model can be chosen (first step for N-L estimation). Several experimental tests, hereafter described, were conducted in the laboratory flotation column. A constant concentration of 10 ppm of frother was used in all tests. Shearing water $J_L$ was varied in steps of 0.2 cm/s, between 0 to 1, and air flow was modified in steps of 0.2 cm/s between 0.5 to 1.5 cm/s. A total of 36 steady-state points were collected. Figure 5.7 depicts the results for $\mu$ and for $\sigma$.

After the tests were carried out, the model for $\mu$ and for $\sigma$ were estimated using a non-linear least squares algorithm. Various mathematical models were tested. For $\mu$, a polynomial was retained.

$$\mu(v_{\mu G}, v_{\mu L}) = 2.815 + 0.1366 v_{\mu G} - 0.1245 v_{\mu L} \tag{5.10}$$

with $R^2$=93.3%. The estimated function for $\sigma$ is:

$$\sigma(v_{\sigma G}, v_{\sigma L}) = 0.1975 + 0.068 e^{(1.105 v_{\sigma G} - 2.011 v_{\sigma L})} \tag{5.11}$$

with $R^2$=98.5%.

The resulting fitting is shown in Figure 5.7. Applying the natural logarithm to equation 5.11 leads to:

$$\ln(\sigma(v_{\sigma G}, v_{\sigma L}) - 0.1975) = -2.688 + 1.105 v_{\sigma G} - 2.011 v_{\sigma L} \tag{5.12}$$

which is a linear function.

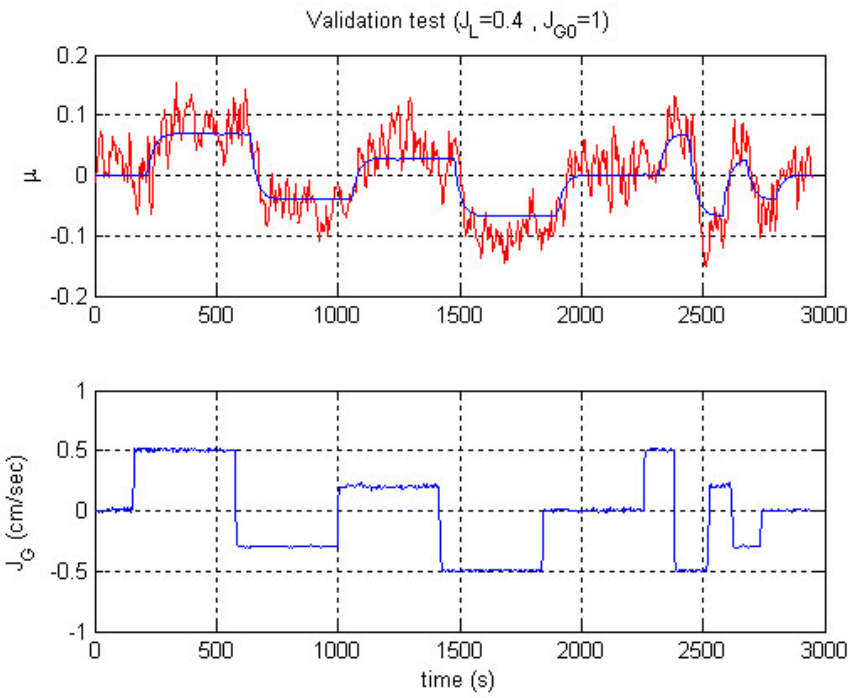


Figure 5.8: Identification results

| **Transfer function** | $\tau$ | $\theta$ |
|---|---|---|
| $G_{j_{G\mu}}$ | 25 ± 2.6 | 57 ±1.9 |
| $G_{j_{G\sigma}}$ | 15 ± 3.4 | 53 ±2.5 |
| $G_{j_{L\mu}}$ | 61 ± 3.6 | 117 ±2.6 |
| $G_{j_{L\sigma}}$ | 43 ± 3.4 | 113 ±2 |

Table 5.3: Identification summary

Subtracting the constant value in equations 5.10 and 5.12 gives,

$$\mu^*(v_{\mu G}, v_{\mu L}) = \mu_0(v_{\mu G}, v_{\mu L}) - 2.815 = 0.1366 v_{\mu G} - 0.1245 v_{\mu L} \tag{5.13}$$

$$\sigma^*(\sigma(v_{\sigma G}, v_{\sigma L}) = \ln(\sigma(v_{\sigma G}, v_{\sigma L}) - 0.1975) - 2.688 = 1.105 v_{\sigma G} - 2.011 v_{\sigma L} \tag{5.14}$$

### BSD linear dynamics

Once the non-linearities were calculated, a series of tests for the identification of the linear dynamic transfer functions were carried out (as detailed in section 5.3). To collect data under different conditions, one variable was kept stable (e.g. $J_g$), while the other ($J_L$) was varied in steps for identification purposes. For the identification of relationship between the shearing water flow rate setpoint and the BSD, air flow rate was stabilized at 0.5 cm/s and a series of step changes were made in shearing water flow. The same series of steps in shearing water

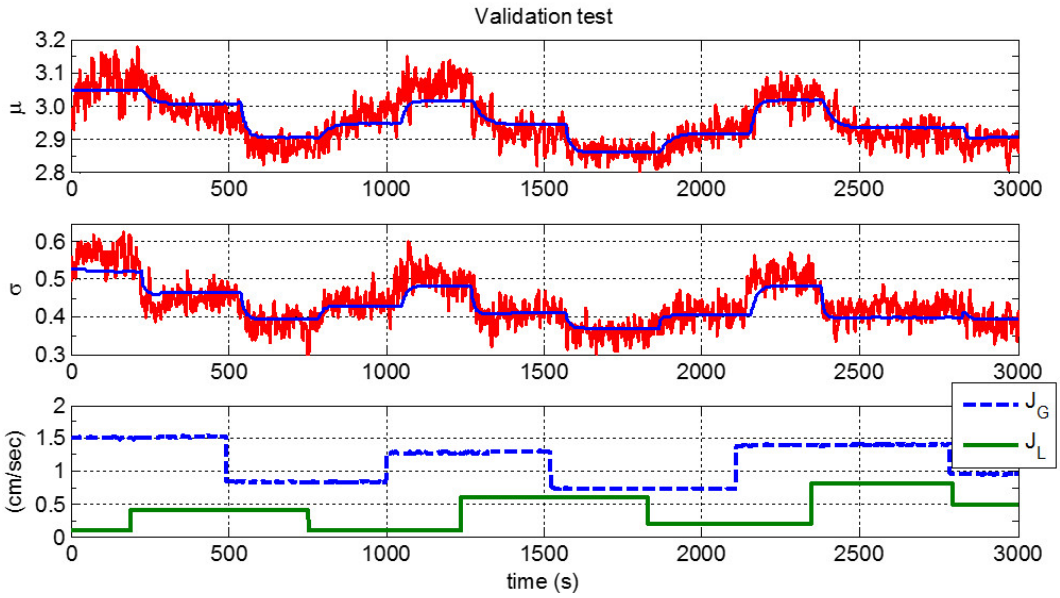


Figure 5.9: Validation test which changes in $J_G$ and $J_L$ in different step series

flow was made for two other air flow rate setpoints (0.9 cm/s and 1.3 cm/s). Same pattern was applied for the identification of the dynamics of BSD by manipulating the air flow rate setpoint. The $J_G$ value was stabilized at 0.0 cm/s, 0.4 cm/s and 0.9 cm/s, and a series of step changes in air flow rate setpoint were made for each $J_G$ value. A total of six sets of dynamic data were thus collected (three for $J_G$ and three for $J_L$). Two of those tests were used for identification while the third was kept for validation purposes. The transfer function variables were identified using a maximum likelihood estimation algorithm. For the four LTI elements, the structure of the model is a first order transfer function with a time delay ($\tau$ is the time constant and $\theta$ is the delay, both variables in seconds). The gain of each transfer function was forced to be equal to one, as previously mentioned in section 5.3. Table 5.3 summarizes the identified parameters for each relationship. Figure 5.8 shows the comparison between the validation test for the relationship between $J_G$ and $\mu$. It must be empathized that validation data is different from the identification data. A reasonable fit was found in all four cases.

After the identification process, another test was made, varying both $J_G$ and $J_L$ in a series of step changes. Figure 5.9 illustrate a validation essay for changes in both variables simultaneously. Again, there is a proper fitting between the test data and the simulated result by using the estimated model. This model was tested under different experimental conditions with reasonable good behavior for all scenarios.

## 5.5 Conclusions

Fitting the BSD by a log-normal distribution shows good results as suggested by previous works. Given the characteristics of the system, a non-linear relationship is found between

the manipulated variables ($J_G$ and $J_L$) and the log-normal parameters ($\mu$ and $\sigma$). A block oriented model, particularly a Wiener structure, has been used in this work for modeling the BSD dynamic, as a result of the wide applicability of this system. The good agreement between the response of the process and the response of the identified model shows the ability of this structure for modeling this type of non-linear processes. If the non-linear elements are invertible, a linear control method can then be implemented. A control strategy design will be explained in chapter 6 aiming at finding the bubble size distribution that optimizes the concentrate recovery for a given particle size or particle size distribution.

# Chapter 6

# Bubble size distribution control in a flotation column[1]

**Abstract** Among the so-called gas dispersion properties affecting flotation column performances, the bubble size distribution (BSD) is one of the most important and its control is crucial to optimize the recovery and grade of the produced concentrate. Experimental tests were carried out in a laboratory flotation column working with air and water, with the objective to regulate the BSD to a desired distribution setpoint. BSD was measured using an image analysis method described in chapter 4. A dynamic model for BSD based on a log-normal distribution was then calibrated. Finally, a model predictive controller (MPC) was designed to control the BSD. The proposed approach leads to good control performances, confirming the possibility to use this strategy to optimize the valuable mineral recovery by adequately selecting the BSD for a given particle size distribution.

**Résumé** Parmi les propriétés de dispersion de gaz affectant les performances des colonnes de flottation, la distribution de la taille des bulles (BSD) est l'une des plus importantes et son contrôle est essentiel pour optimiser la récupération et la teneur du concentré produit. Des essais expérimentaux ont été effectués dans une colonne de flottation de laboratoire opérant avec de l'air et de l'eau, dans le but de réguler la BSD à la cible désirée. La BSD a été mesurée en utilisant une méthode d'analyse d'images, décrite dans le chapitre 4. Un modèle dynamique pour BSD basé sur une distribution log-normale a ensuite été calibré. Enfin, un contrôleur prédictif (MPC) a été conçu pour contrôler la BSD. L'approche proposée conduit à de bonnes performances de contrôle, confirmant la possibilité d'utiliser cette stratégie pour optimiser la récupération de minéraux de valeur en sélectionnant adéquatement la BSD pour une distribution de taille de particule donnée.

[1] A. Riquelme, A. Desbiens, R. del Villar, and M. Maldonado. "Bubble Size Distribution control in a flotation column". This article is in process of submission to the journal Minerals Engineering.

## 6.1 Introduction

Performance in flotation is determined by the grade and recovery of the valuable mineral. Grade is usually measured by an X-ray on stream analyzer (OSA). Recovery can be estimated by a steady state material balance which means that it cannot be used for dynamic control purposes. Moreover OSA devices are designed to sample from different flotation circuits, causing a significant measure delay [37]. This frequently prevents the use of these measurements for online control. Therefore, recovery and grades are often controlled indirectly by instead regulating secondary variables such as gas dispersion properties.

The three main objectives when operating a flotation column are [61]: (1) To stabilize circuit performance by minimizing the frequency and severity of erratic operation, (2) to achieve nominated grade or recovery setpoints, and (3) to maximize the economic performance of the circuit.

The interaction between rising bubbles and particles is the heart of the flotation process. One way to improve the flotation process would certainly to adjust the bubble size distribution in order to optimize the recovery of the particle size distribution [36, 27]. However, to implement this strategy, it is required to measure and control the whole bubble size distribution instead of just an average value. Indeed, an infinite number of distributions can give the same average value but of course they would not lead to the same flotation behavior.

Wishing to control a distribution instead of an average value occurs in many processes such as the flocculent control in paper machines [103], the flame temperature control [87], the molecular weight control in polymerization processes [107], among others. For all these processes, the product quality is better expressed by some variable distribution rather than its mean.

Classical linear stochastic control does not solve the problem of controlling the shape of the distribution instead of their moments [39]. One of the first journal papers about a distribution control strategy was published in 1996 by Kárný [42], where the necessity of controlling the whole distribution rather than just one parameter for stochastic processes was pointed out. Some theoretical structures for the design of the controller were discussed, based on the minimization of the "Kullback-Leibler" distance (a maximum likelihood method), assuming a linear Gaussian state-space model. This approach was theoretical, but provided new guidelines for future research.

Wang et al. [98] indicated that a stochastic distribution control can be classified into three different groups:

- output probability density function control using input-output models;
- minimum entropy control for non-Gaussian stochastic systems;

- output probability density function control using neural networks.

The choice of one of these methods depends principally on how the PDF is modeled. Parametric and semi-parametric methods have been considered when the control of the PDF is desired. The chosen modeling technique is used to compare the process output PDF with the desired PDF and for the controller design.

Forbes et al. [23], parameterizes the PDF using Gram-Charlier (GC) basis functions and calculates the analytical solution for GC components. Then, the target PDF is achieved by the design of a constant feedback gain control.

Another strategy consists in dealing with the probability potential. This concept is driven by Fokker-Planck-Kolmorov (FPK) equations, where a partial differential equation describes the PDF time evolution [16]. This method can be used on systems that can attain the exact desired output PDF in steady-state, leading to impractical feedback control otherwise.

Pigeon et al. [72] critically discuss the GC and the FPK methods to analyze the performance for specific shapes of PDFs, showing that FPK models with ISE minimization gives better results than minimizing the GC coefficients. They also conclude that a switching linear controller has a better performance than a polynomial controller in either case (FPK and GC).

Jian-Qiao [40] proposes a method based on Itô differential equations and stochastic calculus to model stochastic processes. The controller hierarchically regulates the process moment equations. In a case study, the first two moments (mean and standard deviation) are used to generate the control equation.

One alternative to the PDF parametric modeling is investigated by Wang et al. [98]. This method uses B-spline neural networks to calculate a semi parametric decomposition of the PDF. The resulting PDF is a linear combination of a group of B-splines multiplied with a weighting vector [99, 100, 101, 98]. The weights are used to generate a discrete-time ARMAX system, and an optimal control is designed to track the target PDF. This strategy is able to control multimodal distributions since the inclusion of the weight vector can generate practically any distribution in the desired interval [98, 102].

More recently, Maldonado proposed a similar strategy to Wang's, using Gaussian mixture models (GMM) instead of B-splines [50] to represent BSD in flotation. This modeling strategy is a simplified method of GMM assuming fixed means and standard deviations for each kernel component. By doing so, the EM algorithm only has to estimate the weights for each distribution. The problem of controlling the BSD is formulated as an optimization problem whose cost function aims to optimize the geometric distance between the system output and the target distribution.

In this section, a model predictive controller (MPC) will be used to control the bubble size

distribution in a flotation column. A Wiener model was developed for estimating BSD based on a parametric function (log-normal PDF) in chapter 5. A linear model deducted from this Wiener structure will be used to perform the controller predictions.

Section 6.2 introduces the BSD measurement and its nonlinear modeling by a Wiener system structure. Identification results are also detailed in this section. Section 6.3 presents the MPC designed to regulate the mean and variance of BSD. Section 6.4 shows the achieved control results. The last section summarizes the conclusions and the future work.

## 6.2 BSD measurement and modeling

For the design of a model-based control strategy, a model that can predict the BSD from the manipulated variable moves is required. This section explains how the BSD is represented by a log-normal function and it also describes the Wiener dynamic model. Identification results are also summarized. Later, in section 6.4, this model is used to design a control strategy.

### 6.2.1 BSD measurement

As proposed in previous works on flotation mechanical cells and columns, bubble size distributions can be reasonably well fit with log-normal distributions [13, 30, 49]. A log-normal probability density function is defined as

$$P(x) = \frac{1}{\sigma\sqrt{2\pi}x} exp\left[-\left(\ln\left[x-\mu\right]\right)^2/(2\sigma^2)\right] \tag{6.1}$$

where $P(x)$ is the probability density function of the random variable $x$, $\sigma$ is the standard deviation and $\mu$ is the mean.

It is then necessary to find a method to calculate the log-normal parameters that properly represents the measured BSD. A maximum likelihood estimation (MLE) [19] allows to obtain these values by making the modeled data most likely to fit the experimental ones. Riquelme et al. [77], presents a strategy to estimate on-line with a MLE algorithm the parameters $\mu$ and $\sigma$ of a log-normal BSD in a laboratory flotation column. From images taken by a camera, this technique provides the BSD measurement required for the control implementation.

## 6.3 Controller design

The model of the system that is required for the controller to calculate the predictions on the MPC is thus defined in chapter 5. This model is defined by the constant values expressed in equations 5.13 and 5.14, and the dynamics described in table 5.3. The resulting model is shown in figure 6.1. This linear model relates the variables $\mu^*$ and $\sigma^*$ with $J_G$ and $J_L$. The

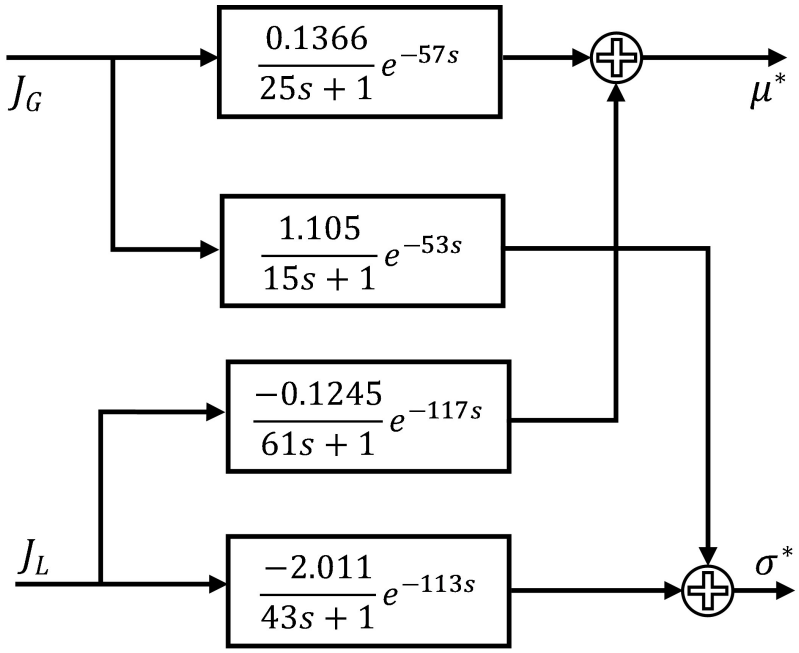


Figure 6.1: Linear model employed to calculate the predictions on the MPC

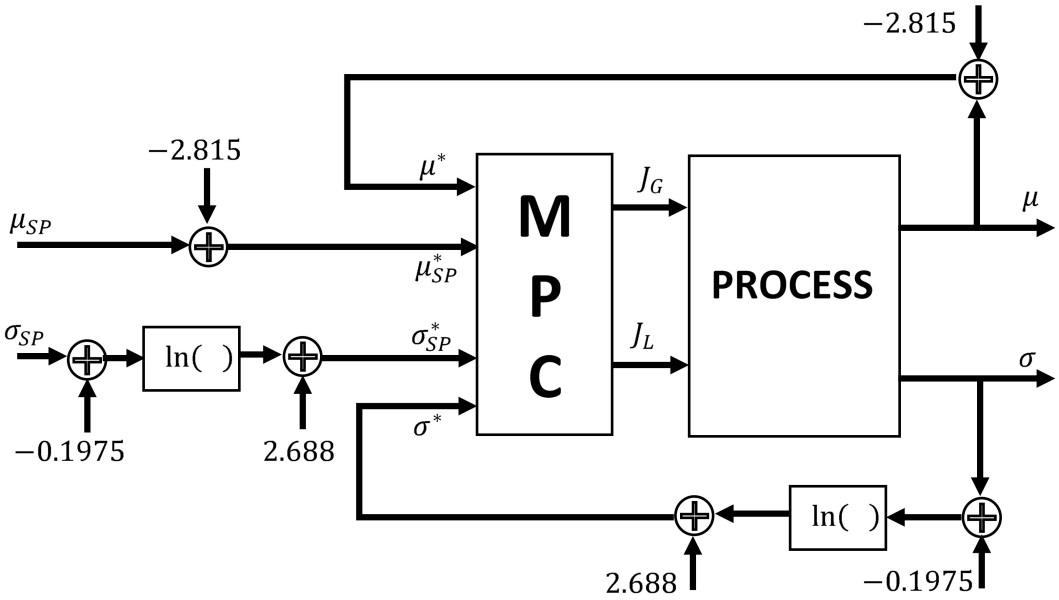


Figure 6.2: Control strategy scheme

procedure to convert the measurements and the setpoints of $\mu$ and $\sigma$ in function of $\mu^*$ and $\sigma^*$ is described in this section.

The control strategy is a constrained multi-input/multi-output (MIMO) model predictive controller (MPC). Figure 6.2 shows the MPC and the mathematical operations to convert the structure in a lineal system as expressed by equations 5.13 and 5.14. The MPC was

implemented via Matlab MPC toolbox. The objective is to control $\mu^*$ and $\sigma^*$ by manipulating $J_G$ and $J_L$. By consequence, the desired $\mu$ and $\sigma$ can be attained. The model parameters employed to perform the predictions are shown in Figure 6.1. The main advantage of this approach is that calculating the predictions with a linear model simplifies the design of the controller.

The control action are obtained by solving at each sample time the following optimization problem:

$$\min_{\Delta u(k|k)\ldots\Delta u(H_C-1+k|k)} \sum_{i=0}^{H_p-1} \Big( \big(\widehat{y}_j(k+i+1 \mid k) - r_j(k+i+1)\big)^T w^y \big(\widehat{y}_j(k+i+1 \mid k) - r_j(k+i+1)\big) + \big(\Delta u_j(k+i \mid k)\big)^T w^{\Delta u} \big(\Delta u_j(k+i \mid k)\big) \Big) + \rho\, e^2 \tag{6.2}$$

subject to the following constraints:

$$u_{min}(i) \leq u(k+i \mid k) \leq u_{max}(i) \tag{6.3}$$

$$y_{min}(i) - e \leq y(k+i \mid k) \leq y_{max}(i) + e \tag{6.4}$$

$$\Delta u(k+h \mid k) = 0, h = H_c, \ldots, H_p - 1 \tag{6.5}$$

where:

- $H_c$ and $H_p$ are respectively the control and prediction horizon and the operator $(\cdots)^T$ denotes the vector transpose,
- $\widehat{y}(k+i \mid k) = \begin{bmatrix} \widehat{\mu^*}(k+i \mid k) \\ \widehat{\sigma^*}(k+i \mid k) \end{bmatrix}$. These are the predictions of the two system outputs ($\mu^*$ and $\sigma^*$), for the instant $k+i$ calculated at the current time $k$,
- $r$ are the setpoints over the prediction horizon (assumed equal to the current references): $r(k+i) = r(k) = \begin{bmatrix} \mu^*_{SP}(k) \\ \sigma^*_{SP}(k) \end{bmatrix}$,
- $\Delta u$ is the variation of each manipulated variable: $\Delta u(k) = \begin{bmatrix} J_G(k) - J_G(k-1) \\ J_L(k) - J_L(k-1) \end{bmatrix}$,

| Transfer function | Weight |
|---|---|
| $w_{JG}$ | 0.4 |
| $w_{JL}$ | 0.2 |
| $w_{\mu}$ | 8 |
| $w_{\sigma}$ | 1 |

Table 6.1: Weights on manipulated and controlled variables

| Variable | Unit | Minimum | Maximum |
|---|---|---|---|
| $J_G$ | cm/s | 0.5 | 2 |
| $J_L$ | cm/s | 0 | 1 |
| $\mu^*$ | - | -0.0658 | 0.3012 |
| $\sigma^*$ | - | -0.6232 | 1.7312 |

Table 6.2: Constraints for manipulated and controlled variables

- $w^y$ is the weight for the output variables, i.e. $w^y = \begin{bmatrix} w_{\mu} & 0 \\ 0 & w_{\sigma} \end{bmatrix}$,
- $w^{\Delta u}$ is the weight for the variations of the manipulated variables, i.e. $w^{\Delta u} = \begin{bmatrix} wJG & 0 \\ 0 & w_{JL} \end{bmatrix}$.

Also, there is one "slack" variable $e$ used to relax the constraints imposed to the controlled variables (equation 6.4). The weight $\rho$ in the last term in equation 6.2 penalizes the violation of constraints [64] and is calculated as

$$\rho = 10^5 \max\{w^y, w^{\Delta u}\} \tag{6.6}$$

The MPC was tuned aiming at having closed-loop dynamics similar to the process dynamics. This usually leads to a robust controller. The control interval was set at 2 seconds in order to allow the overall dynamics to properly reject disturbances. As a consequence of the choice of the control interval, the prediction horizon $H_p$ was set to 40 control intervals and the control interval $H_c$ was set to one sampling time. Table 6.1 summarizes the weights for the manipulated and the controlled variables. Weights were tuned by a trail-and-error procedure seeking the desired dynamics.

Matlab MPC observer is a Kalman filter. This observer is designed to provide estimates of the states of the plant model to calculate the output predictions at each control interval. In order to properly reject a constant output disturbance, the overall process model is augmented by a disturbance model consisting of an integrator driven by white noise for each output. The observer gains were tuned empirically aiming to a fast estimation of the model states.

Table 6.2 summarizes the variable constraints. For the case of the output variables, minima and maxima are extreme values for keeping the system in an appropriate operation zone. The

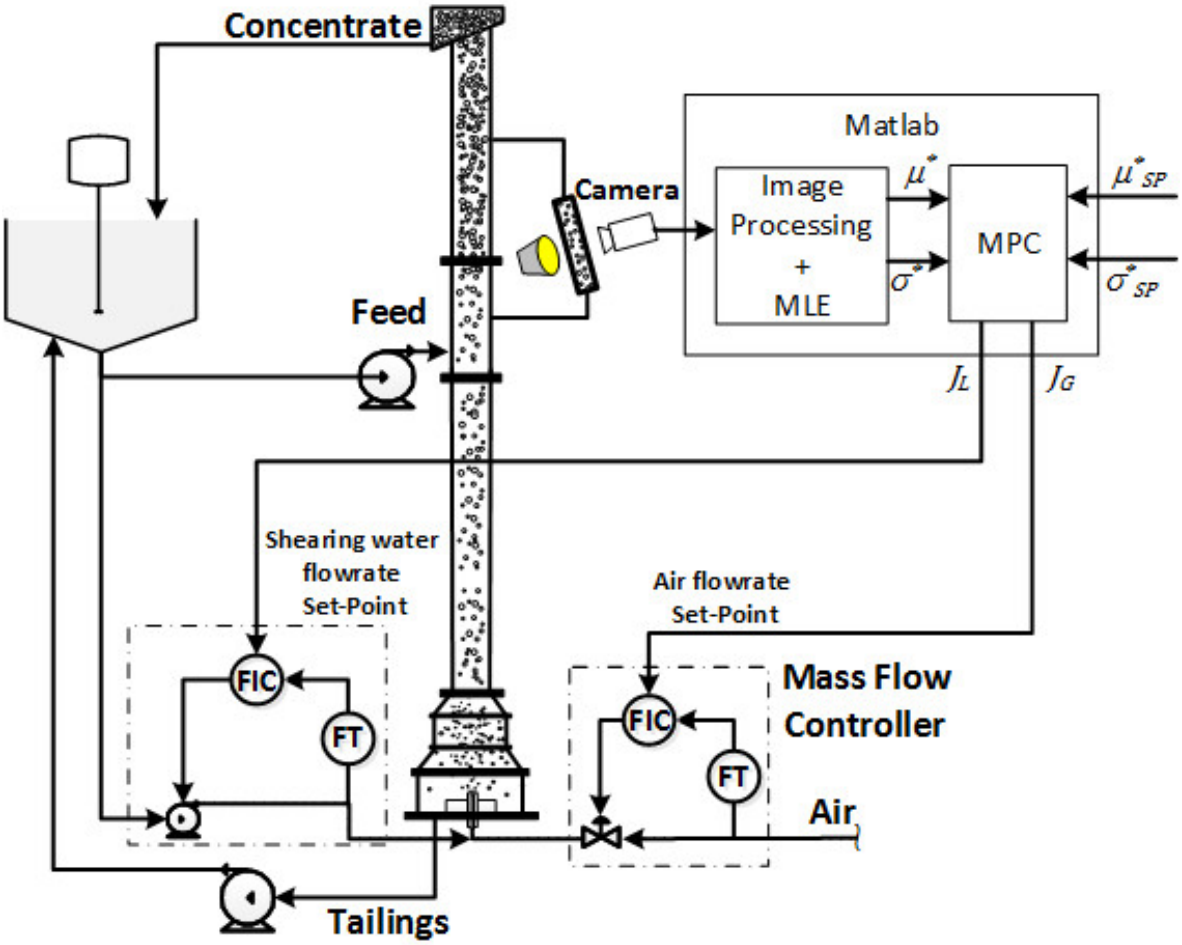


Figure 6.3: Laboratory column set-up

minimum $J_G$ warranties a minimum bubble generation, while its maximum value prevents operating the column in a bubbly zone [22]. $J_L$ values greater than the maximum limit do not change the variables $\mu$ and $\sigma$ significantly.

## 6.4 Results

Figure 6.3 shows the column configuration. The method proposed in chapter 5 was used to calculate the lognormal parameters $\mu$ and $\sigma$, while the variables $\mu^*$ and $\sigma^*$ were calculated by applying equations 5.13 and 5.14. Refer to figure 6.2 for more details about the controller.

The designed controller was implemented on the laboratory flotation column for its validation. Figure 6.4 shows the obtained results. During the first 400s the process was operated in open loop until the variables were stabilized for a proper switching from manual to automatic mode. Between 400s and 2800s several setpoint changes were made, both on $\mu$ and $\sigma$. In all cases the control system showed a very good performance. After the 2800s two changes on the setpoint

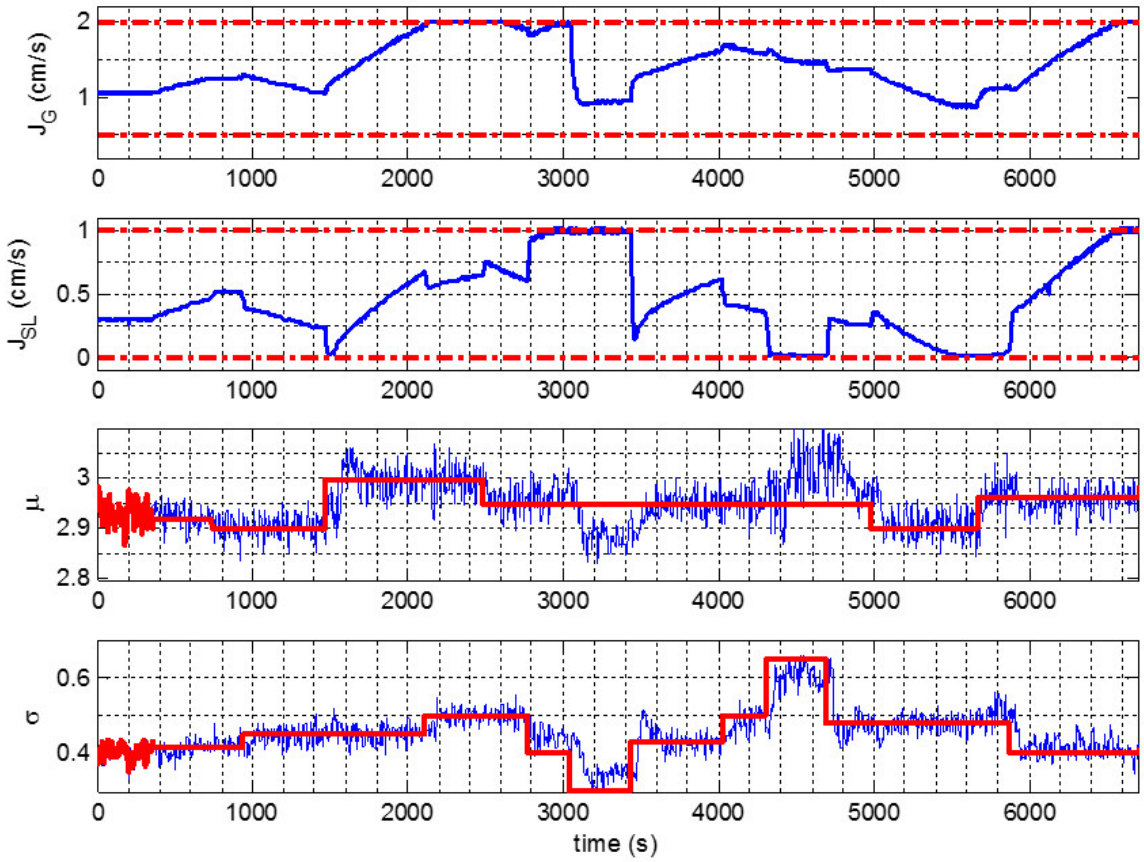


Figure 6.4: Control results

of $\sigma$ were made thereby saturating the manipulated variable $J_L$ at 1. At 3000s, it is possible to observe that the value of $\mu$ is decreased by the controller to compensate the error produced by the saturation of shearing water at 1cm/s. The same situation is observed at 4200s, where the shearing water flow rate was saturated at its minimum value, generating again (as at the 2800s) a static error in both output variables. As expected, they are not a significant impact between the controlled variables for individual reference changes, and the constraints for the manipulated variables are respected.

## 6.5 Conclusions

This paper described the design of a constrained MIMO MPC strategy for controlling the bubble size distribution in a flotation column. The controller predictions are calculated with a linear model deducted from a non-linear Wiener system. Laboratory results shows that the MPC is able to control the process with adequate dynamics while respecting constraints.

The final goal of this research is to control at the same time the BSD and the bubble surface area flux (BSAF). BSAF is defined as the ratio between the superficial air rate $J_G$ and the

Sauter mean diameter $D_{32}$ [47]. It has been proved that different BSD can produce the same $D_{32}$ [50], therefore the same BSAF. Controlling the shape of the BSD and BSAF at the same time is a required step in order to find the BSD that optimizes the recovery given a specific PSD. As proposed by Maldonado (2010b), keeping BSAF at a desired value while BSD is controlled can be introduced in the controller (MPC) optimization problem as a linear equality constraint.

It was shown that the frit-and-sleeve sparger allows the control of the BSD. However, it was observed that it is not possible to generate a wide range of means and standard deviations. Having more than one frit-and-sleeve spargers working at the same time in the column, each of them with different characteristics, would help generating various BSD. This would introduce a new challenge in the identification of the log-normal parameters of a mixture model as well detecting the contribution of each sparger in the total BSD.

During the experimental tests, the frother concentration was kept constant, although this variable has a significant impact on bubble size. Maldonado [53] designed a multi-model approach to estimate frother concentration in a laboratory flotation column. Finding a control strategy to continuously (on-line) modify the frother concentration could add another degree of freedom in controlling the BSD, or the BSAF.

# Conclusion and future work

The main objective of this work was the development of a strategy to control the bubble size distribution (BSD) in a laboratory flotation column. This objective was attained as indicated in chapter 6. A model predictive controller was designed to achieve a desired BSD by the manipulation of two flow rates available in the sparging device (shearing water and gas). To reach this objective, previous steps were developed and described separately in chapters 3, 4 and 5. The purpose of the present section is to summarize and unify the conclusions of each chapter while providing as well some suggestions for future work.

Chapter 2 describes a low-cost circuit designed to measure electrical conductivities in an extended rage of values usually encountered in the minerals processing pulps. This device was later implemented for the estimation of three important secondary variables of flotation: froth depth, gas hold-up and bias rate. A major improvement in the measurement of these variables is observed. The control of froth depth, via a PI controller, and of gas hold-up and bias, through a two-by-two model predictive controller, using this measurement device was later developed by Calisaya et al. [9, 10].

The development of a new measurement technique to estimate the BSD is explained in Chapter 4. This technique is based on an image processing algorithm for on-line detection and measurement of bubbles' sizes from a set of pictures taken in a Bubble Viewer. The Circular Hough Transform is applied on each picture to detect the bubbles captured on the image. By applying this transform, the adjustment of the detection of less perfectly-circular bubbles becomes possible. This characteristic is crucial for identifying large bubbles and clustered bubbles (whether composed of just small bubbles or a large bubble carrying small ones with it). Compared to the previously employed method, which detects just circular bubbles (circular particle detection algorithm), this technique largely improves the measurement of the whole BSD. By using this new approach, an error of 3% on the estimation of the Sauter mean diameter was observed compared to 18% error with the previous algorithm.

Chapter 5 explains how the measurement technique previously mentioned is employed to design a dynamic model of BSD. As proposed in previous works, the BSD is well represented by a log-normal distribution. A series of identification tests were carried-out to find the relationship between the log-normal parameters (mean and standard deviation) and the manipulated

variables (shearing water and flow rate setpoints). Given the nonlinear relationship existing between these variables, a Wiener model was implemented. The nonlinear elements were modeled considering invertible functions aiming at the design of a control strategy. An accurate fitting between the process and the model was observed.

Finally, Chapter 6 describes the design of a BSD control strategy. A constrained MIMO MPC was design by using the Wiener model calibrated in the previous chapter. This was possible by inverting the nonlinear elements of the Wiener model. The desired performance for controlling the shape of the BSD was attained, i.e. approximately the same dynamics as in open loop.

### 6.5.1 Future work

The following topics are suggested for further studies:

- Industrial application of the bubble size measurement algorithm proposed in Chapter 4. This work should be preceded by three-phase (bubbles, water and particles) laboratory tests. A bubble viewer, e.g. that has been developed by McGill researchers, should be adapted for continuously work with solids. Implementing an automated system of washing the viewing chamber will be required, such as that proposed by Roy [81].

- The manipulation of the frother concentration as another degree of freedom to control BSD. The on-line measurement of this manipulated variable is possible using the technique proposed by Maldonado [51]. A dynamic model including the frother concentration as a manipulated variable seems an interesting field to be investigated.

- The BSD modeling for the case of multiple frit-and-sleeve spargers. Since the porosity of the porous ring and the gap sleeve can be modified in the frit-and-sleeve sparger, different bubble sizes distributions could be generated by adding more spargers. The challenge lies in the conception of a dynamic model between the generated distribution of each sparger and its manipulated variables (i.e. shearing water and air flow rates of each sparger).

- Applications of bubble size distribution control in a laboratory flotation column by manipulating multiple frit and sleeve spargers.

- Beware that now is able to control the BSD, an obvious outcome would be to study the relation between the BSD and the particle size distribution for optimum metallurgy (concentrate grade and recovery).

# Appendix A

# Sensitivity analysis for oscillator components

Sensitivity analysis of $\tau - \tau_0$ (the variable required to estimate $K_e$ according to equation 3.4) is carried out based on equation 3.1. The sensitivity of $\tau - \tau_0$ for variations of $R_e$ is:

$$S_{R_e}^{\tau-\tau_0} = \frac{\delta(\tau - \tau_0)}{\delta R_e} \cdot \frac{R_e}{\tau - \tau_0} = 1. \tag{A.1}$$

As expected, $\tau - \tau_0$ only depends on the value of $R_e$ and not on $R_s$. This is confirmed calculating the sensitivity of $\tau - \tau_0$ for variations of $R_s$:

$$S_{R_s}^{\tau-\tau_0} = \frac{\delta(\tau - \tau_0)}{\delta R_s} \cdot \frac{R_s}{\tau - \tau_0} = 0. \tag{A.2}$$

For the capacitor, the sensitivity of $\tau - \tau_0$ for variations of $C$ is:

$$S_{C}^{\tau-\tau_0} = \frac{\delta(\tau - \tau_0)}{\delta C} \cdot \frac{C}{\tau - \tau_0} = 1. \tag{A.3}$$

This dependence is useful for choosing the desired range of measurable resistance, as explained in section 5.

# Bibliography


[1] Imagej (version 1.46) [computer software].

[2] N. Ahmed and G. Jameson. The effect of bubble size on the rate of flotation of fine particles. *International Journal of Mineral Processing*, 14(3):195–215, 1985.

[3] E-W. Bai. A blind approach to the Hamerstein-Wiener model identification. *Automatica*, 38:967–979, 2002.

[4] E-W. Bai. Frequency domain identification of Wiener models. *Automatica*, 39:1521–1530, 2003.

[5] S. Banisi, J. Finch, and A. Laplante. Electrical conductivity of dispersions: A review. *Minerals Engineering*, 6(4):369–385, 1993.

[6] G. Barral, J. Diard, B. Le Gorrec, and C. Tri, L. ; Montella. Impedance of conductivity cells. determination of the measurement frequency range of the conductivity. *Journal of Applied Electrochemistry*, 15(6):913–1924, 1985.

[7] C Bishop. *Pattern recognition and machine learning*. Springer-Verlag, 2006.

[8] S. Boyd and L. Chua. Fading memory and the problem of approximating nonlinear operators with Volterra series. *IEEE Transactions on Circuits and Systems*, 32(11):1150–1161, 1985.

[9] D. Calisaya, E. Poulin, A. Desbiens, R. Del Villar, and A. Riquelme. Multivariable predictive control of a pilot flotation column. *Proceedings of the American Control Conference*, 1:4022–4027, 2012.

[10] D. Calisaya, A. Riquelme, E. Poulin, A. Desbiens, and R. Del Villar. Constrained multivariable control of a pilot flotation column at the laronde concentrator. *Proceedings of Annual Conference of the Canadian Mineral Processors*, 1:169–181, 2012.

[11] R. Cardenas-Dobson, S. Serpa, S. Villegas, and J. Retamales. Conductivity sensor for mining applications. *IMTC/98 Conference Proceedings. IEEE Instrumentation and Measurement Technology Conference*, 2:1050–1055, 1998.

[12] A. Cervantes, O. Agamennoni, and J. Figueroa. A nonlinear model predictive control system based on Wiener piecewise linear models. *Journal of Process Control*, 13:655–666, 2003.

[13] Z. Chen, C. Zheng, Y. Feng, and H. Hofman. Local bubble behavior in three-phase fluidized beds. *The Canadian Journal of Chemical Engineering*, 76:315–318, 1998.

[14] T. Cienski and V. Coffin. Column flotation operation at mines Gaspé molybdenum circuit. *Proceedings of the 13th annual meeting of the Canadian mineral processors, CIM*, 1:240–262, 1981.

[15] B. Clingan and D. McGregor. Column flotation experience at Magma Copper Co. *Minerals and metallurgical processing*, 3:121–125, 1987.

[16] L. G. Crespo and J. Q. Sun. Nonlinear stochastic control via stationary probability density functions. *Proceedings of the American Control Conference*, 3:2029–2034, 2002.

[17] R. da Rocha, I. Gutz, and C. do Lago. A low-cost and high-performance conductivity meter. *Journal of Chemical Education*, 74(5):572, 1997.

[18] M. Daraei, J. Rezaie, N. Norouzi, and A. Khajooeizadeh. An innovative implementation of circular Hough transform using eigenvalues of covariance matrix for detecting circles. *International Symposium Electronics in Marine*, 1:397–400, 2011.

[19] A. P. Dempster, N. M. Laird, and D. B Rubin. Maximum likelihood from incomplete data via the em algorithm. *Journal of the Royal Statistical Society*, 39(1):1–38, 1977.

[20] R. Duda and E. Hart. Use of the Hough transformation to detect lines and curves in pictures. *Communications of the ACM*, 1:11–15, 1972.

[21] E. Ferrara, L. Callegaro, and F. Durbiano. Optimal frequency range for the measurement of A.C. conductivity in aqueous solutions. *Instrumentation and Measurement Technology Conference*, 2:775 – 779, 2000.

[22] J. Finch and G. Dobby. *Column flotation*. Pergamon Press, 1990.

[23] M. G. Forbes, M. Guay, and J. F. Forbes. Control design for first-order processes: shaping the probability density of the process state. *Journal of Process Control*, 4:399–410, 2004.

[24] C. Gomez, F. Cortes-Lopez, and J. Finch. Industrial testing of a gas holdup sensor for flotation systems. *Minerals Engineering*, 16(6):493–501, 2003.

[25] C. O. Gomez and J. A. Finch. Gas dispersion measurements in flotation cells. *International Journal of Mineral Processing*, 84:51–58, 2007.

[26] J. Gomez and E Baeyens. Subspace identification of multivariable Hammerstein and Wiener models. *European Journal of Control*, 11:1–10, 2005.

[27] B. Gorain, J.-P. Franzidis, and E. Manlapig. Studies on impeller type, impeller speed and air flow rate in industrial scale flotation cell. part 4: Effect of bubble surface area flux on flotation performance. *Minerals Engineering*, 12(8):1557–1570, 1995.

[28] J. Goulermas and P Liatsis. Novel combinatorial probabilistic Hough transform technique for detection of underwater bubbles. *Proceedings of Machine Vision Applications in Industrial Inspection*, 3029:147–156, 2012.

[29] J. Graeme and G. Tobey. *Operational Amplifiers. Design and Applications*. McGraw-Hill book company, 1971.

[30] R. Grau and K. Heiskanen. Bubble size distribution in laboratory scale flotation cells. *Minerals Engineering*, 18(12):1164–1172, 2005.

[31] M. Gregoire. Instrumentation et contrôle automatique d'une colonne de flottation de laboratoire. Master's thesis, Dept. of Electrical Engineering, Laval University, Quebec (Canada), 1997.

[32] R. Haber and H. Unbehauen. Structure identification of nonlinear dynamic system, a survey on input/output approaches. *Automatica*, 26(4):651–677, 1990.

[33] A. Hagenblad, L. Ljung, and A. Wills. Maximum likelihood identification of Wiener models. *Automatica*, 44:2697–2705, 2008.

[34] M. Han, Y. Park, and T Yu. Development of a new method of measuring bubble size. *Water Science and Technology: Water Supply*, 2(2):77–83, 2002.

[35] P. Hawkins. A low-powered resistance and conductivity measuring circuit for use with remote transducers. *Measurement Science & Technology*, 1(9):845–847, 1990.

[36] K. Heiskanen. On the relationship between flotation rate and bubble surface area flux. *Minerals Engineering*, 13(2):141–149, 2000.

[37] P. Holtham and K. Nguyen. On line analysis of froth surface in coal and mineral flotation using jkfrothcam. *International journal of mineral processing*, 64:163–180, 2002.

[38] I. Iqbal and N. Aziz. Comparison of various Wiener model identification approach in modeling nonlinear process. *3rd Conference on Data Mining and Optimization*, 1:134–140, 2011.

[39] A. Jazwinski. *Stochastic process and filtering theory*, volume 64. Mathematics in Science and Engineering, 1970.

[40] S. Jian-Qiao. *Stochastic Dynamics and control: Volume 4*. Elsevier Editorial system, 2006.

[41] R. Jones. Measurements of the electrical conductivity of water. *IEEE Proceedings, Science, Measurement and Technology*, 149(6):320 – 322, 2002.

[42] M. Kárný. Towards fully probabilistic control design. *Automatica*, 32(12):1719–1722, 1996.

[43] S. Kjeldgaard. Circular Hough transform. Technical report, Aalborg University, Vision, Graphics, and interactive systems, 2007.

[44] W. Kratch, C. Gomez, and J. Finch. Controlling bubble size using a frit and sleeve sparger. *Minerals Engineering*, 21(9):660–663, 2008.

[45] J. Lario-Garcia and R. Pallas-Areny. Constant-phase element identification in conductivity sensors using a single square wave. *Sensors and Actuators, A: Physical*, 132:122–128, 2006.

[46] H. Laurila, J. Karesvuori, and O. Tiili. Strategies for instrumentation and control of flotation circuits. *Mineral Processing Plant Design, Practise and Control*, 1:2174–2195, 2002.

[47] J. Leiva, L. Vinnett, F. Contreras, and J Yianatos. Estimation of the actual bubble surface area flux in flotation. *Minerals Engineering*, 23:888–894, 2010.

[48] B. Lin, B. Recke, J. Knudsen, and S. Jorgensen. Bubble size estimation for flotation processes. *Minerals Engineering*, 21(7):539–548, 2007.

[49] S. Majumder, G. Kundu, and D. Mukherjee. Bubble size distribution and gas-liquid interfacial area in a modified downflow bubble column. *Chemical Engineering Journal*, 122:1–10, 2006.

[50] M. Maldonado. *Advances in estimation and control for flotation columns*. PhD thesis, Université Laval, Department of Electrical and Computer Engineering, Université Laval, Quebec, 2010.

[51] M. Maldonado, A. Desbiens, and R. del Villar. An update on the estimation of the froth depth using conductivity measurements. *Minerals Engineering*, 21(12-14):856–860, 2008.

[52] M. Maldonado, A. Desbiens, and R. Del Villar. Potential use of model predictive control for optimizing the column flotation process. *International Journal of Mineral Processing*, 93:26–33, 2009.

[53] M. Maldonado, A. Desbiens, R. del Villar, and R. Aguilera. On-line estimation of frother concentration for flotation processes. *48th Annual Conference of Metallurgists*, 1:135–146, 2010.

[54] M. Maldonado, A. Desbiens, R. del Villar, and J. Chirinos. On-line bias estimation using conductivity measurements. *Minerals Engineering*, 21:851–855, 2008.

[55] M. Maldonado, A. Desbiens, R. del Villar, E. Girgin, and C. Gomez. On-line estimation of bubble size distributions using gaussian mixture models. *Proceedings of 5th International Mineral Processing Seminar: Procemin 2008*, 1:389–398, 2008.

[56] M. Maldonado, A. Desbiens, R. del Villar, E. Poulin, and A. Riquelme. Non-linear control of bubble size in a laboratory flotation column. *Proceedings of 13th Symposium in automation in mining, mineral & metal processing*, 1:33–38, 2010.

[57] M. Maldonado, A. Desbiens, E. Poulin, R. del Villar, and A. Riquelme. Control of bubble size in a laboratory flotation column. *Proceedings of Copper*, 7:2829–2844, 2010.

[58] M. Maldonado, A. Desbiens, E. Poulin, R. del Villar, and A Riquelme. Automatic control of bubble size in a laboratory flotation column. Submitted to the International Journal of Mineral Processing, July 2014.

[59] E. Matiolo, F. Testa, J. Yianatoss, and J. Rubio. On the gas dispersion measurements in the collection zone of flotation columns. *International Journal of Mineral Processing*, 99:78–83, 2011.

[60] J. Maxwell. *A Treatise of Electricity and Magnetism. 3rd Edition.* Oxford University Press, London, 1892.

[61] D. McKee. Automatic flotation control  a review of 20 years on effort. *Minerals engineering*, 4:653–666, 1991.

[62] G. Mercer. A low-cost, portable, and safe apparatus for lecture hall conductivity demonstration. *Biennial Conference on Chemical Education*, 68(7):619–620, 1990.

[63] T. Miettinen, J. Ralston, and D. Fornasiero. The limits of fine particle flotation. *Minerals Engineering*, 23(5):205–223, 2010.

[64] H. Mukai and E. Polak. A second-order method for the general nonlinear programming problem. *Journal of optimization theory and applications*, 26(4):515–532, 1978.

[65] O. Nelles. *Nonlinear System Identification: From Classical Approaches to Neural Networks and Fuzzy Models.* Springer editorial, 2001.

[66] A Nguyen and S. Kmet. Collision efficiency for fine mineral particles with single bubble in a countercurrent flow regime. *International Journal of Mineral Processing*, 35(3):205–223, 1992.

[67] M. Nostrati and R. Karimi. Detection of circular shapes from impulse noisy images using median and laplacian filter and circular Hough transform. *International Conference on Electrical Engineering, Computing Science and Automatic Control*, 1:1–5, 2011.

[68] T Ogunfunmi. *AdaptiveNnonlinear System Identification: The Volterra and Wiener Model Approaches.* Springer editors, 2007.

[69] R. Padma, R. Raghavendra, and K. Subbarangaiah. A simple technique for a.c. conductivity measurements. *Bulletin of Materials Science*, 25(7):647–651, 2002.

[70] H. Park and J. Lee. Simple approaches for the identification of Wiener-type nonlinear process. *5th Asian Control Conference*, 1:93–103, 2004.

[71] T. Peng, A. Balijepalli, S. Gupta, and T. LeBrun. Algorithms for on-line monitoring of micro spheres in an optical tweezers-based assembly cell. *Journal of Computing and Information Science in Engineering*, 7(4):330–339, 2007.

[72] B. Pigeon, M. Perrier, and B. Srinivasan. Shaping probability density functions using a switching linear controller. *Journal of Process Control*, 21:901–908, 2011.

[73] A. Rajendran and P. Neelamegam. Measurement of conductivity of liquids using AT89C55WD microcontroller. *Measurement*, 35(1):59–63, 2004.

[74] D. Ramirez and S. Casans. An analog electronic interface to measure electrical conductivity in liquids. *Measurement*, 38(3):181–187, 2005.

[75] M. Rehman, V. Murti, and M. Gupta. A novel precision type liquid conductivity measuring system. *Journal of Physics E (Scientific Instruments)*, 18(11):902–903, 1985.

[76] A. Riquelme, J. Bouchard, A. Desbiens, and R. del Villar. Bubble detection in flotation columns based on circular Hough transform. *World Mining Congress*, 1:2–10, 2013.

[77] A. Riquelme, J. Bouchard, A. Desbiens, and R. del Villar. Parameterization of bubble size distribution in flotation columns. *16th IFAC Symposium on Control, Optimization and Automation in Mining, Minerals and Metal Processing*, 15(1):128–133, 2013.

[78] A. Riquelme, A. Desbiens, R. del Villar, and M. Maldonado. A device for measuring conductivity of dispersions. *Measurements*, 59:49–55, 2014.

[79] R. Rodrigues and J. Rubio. New basis for measuring the size distribution of bubbles. *Minerals Engineering*, 16:757–765, 2003.

[80] L. Rosenthal. Conductivity measurement method by means of multivibrator frequency control. *Industrial and Engineering Chemistry, Fundamentals*, 16(4):483–486, 1977.

[81] J. Roy. Investigation sur l'impact de la concentration de moussant dans un système solide-liquide-gaz et automatisation d'un capteur de dimension des bulles. Master's thesis, Université Laval, 2013.

[82] J. Russ. *The image processing handbook*. CRC press, 3rd. ed. edition, 1998.

[83] P. Sahoo, N. Malathi, K. Praveen, R. Ananthanarayanan, A. Arun, N. Murali, and P. Swaminathan. High performance conductivity monitoring instrument with pulsating sensor. *Review of Scientific Instruments*, 81(6):065109–1, 7, 2010.

[84] D. Sbarbaro and R. del Villar. *Advanced Control and Supervision of Mineral Processing Plants (Advances in Industrial Control)*. Springer London Ltd., 2010.

[85] Y. Shiotani and Kobayashi. Identification of multi-input multi-output Wiener-type nonlinear system. *ICCAS-SICE International joint conference*, 1:5244–5249, 2009.

[86] P. Soille. *Morphological image analysis: Principles and applications*. NY: Springer-Velag, 2003.

[87] X. Sun, H. Yue, and H. Wang. Modelling and control of flame temperature distribution using probability density function shaping. *Transactions of the Institute of Measurement and Control*, 28(5):401–408, 2006.

[88] S. Sung. System identification method for Hammerstein processes. *Industrial and Engineering Chemistry Research*, 41(17):4295–4302, 2002.

[89] F. Tavera, R. Escudero, C. Gomez, and J. Finch. Determination of solids holdup in thickeners from measurement of electrical conductivity using flow cells. *Minerals Engineering*, 11(3):233–241, 1998.

[90] J. Taylor. *Statistical Techniques for Data Analysis*. Lewis Publishers, 1990.

[91] D. M. Titterington, A. F. Smith, and U. E. Makov. *Statistical analysis of finite mixture distributions*. John Wiley & Sons Inc, UK, 1985.

[92] S. Totterman and H. Toivonen. Support vector method for identification of wiener models. *Journal of Process Control*, 19:1174–1181, 2002.

[93] R. Tremblay and P Boutin. Method and apparatus for the separation and recovery of ores., 1964.

[94] A. Uribe-Salas, C. Gomez, and J. Finch. Conductivity technique for gas and solids holdup determination in three-phase reactors. *Chemical Engineering Science*, 49(1):1–10, 1994.

[95] A. Uribe-Salas, M. Leroux, C. Gomez, J. Finch, and B. Huls. A conductivity technique for level detection in flotation cells. *Proceedings of International Conference on Column Flotation*, 2:467–478, 1991.

[96] J. Vergouw, J. Anson, R. Dalhke, Z. Xu, C. Gomez, and J.A. Finch. Automated data acquisition technique for settling tests. *Minerals Engineering*, 10(10):1095–1105, 1997.

[97] L. Vinnett, F. Contreras, and J. Yianatos. Gas dispersion pattern in mechanical flotation cells. *Minerals Engineering*, 26:80–85, 2012.

[98] A. Wang, H. Wang, and L. Guo. Advances in stochastic distribution control. *10th International Conference on Control, Automation, Robotics and Vision*, 1:1479–1483, 2008.

[99] H. Wang. Robust control of the output probability density functions for multivariable stochastic systems with guaranteed stability. *IEEE Tansactions on Automatic Control*, 44(11):2103–2107, 1999.

[100] H. Wang. *Bounded dynamic stochastic systems. Modelling and control.* Springer-Verlag, New York, 2000.

[101] H. Wang. Minimum entropy control of non-gaussian dynamic stochastic systems. *IEEE Tansactions on Automatic Control*, 47(2):398–403, 2002.

[102] Y. Wang and S. Boyd. Performance bounds for linear stochastic control. *Systems & Control Letters*, 58(3):178–182, 2009.

[103] Y. Yi, L. Guo, and H. Wang. Constrained pi tracking control for output probability distributions based on two-step neural networks. *IEEE Transactions on neural networks*, 56:1416–1426, 2011.

[104] J. Yianatos and F. Contreras. On the carrying capacity limitation in large flotation cells. *Canadian Metallurgical Quarterly*, 4(8):345–352, 2010.

[105] J. Yianatos, J. Finch, and A. Laplante. The cleaning action in column flotation froths. *Trans. Of the institution of mining and metallurgy*, 96:199–205, 1987.

[106] Z. Yu and B. Zhou. A conductivity measurement system based on high-speed A/D peak sampling. *Proceedings of the Third International Conference on Information and Computing Science*, 1:143–146, 2010.

[107] H. Yue, J. Zhang, H. Wang, and L. Cao. Shaping of molecular weight distribution using b-spline based predictive probability density function control. *Proceeding of the 2004 American Control Conference*, 4:3587–3529, 2004.

[108] Y. Zhu, Y. Wu, and R. Manasseh. Rapid measurement of bubble size in gaz-liquid flows using a bubble detection technique. *Australasian Fluid Mechanics Conference*, 1:541–544, 2001.